Performance of Vented Round Parachutes

Project Number: ME-DJO-0407

A Major Qualifying Project Report

Submitted to the Faculty of the

WORCESTER POLYTECHNIC INSTITUTE

in partial fulfillment of the requirements for the

Degree of Bachelor of Science

in Mechanical and Aerospace Engineering

by

Brian Brighenti (AE)

_____

Shawn Duffen (AE)

_____

Kelly Head (MEAE)

_____

Date Submitted

Approved:

_____

Prof. David J. Olinger

Abstract

The purpose of this Major Qualifying Project was to measure the glide ratio of round parachute canopies with various vent areas and materials. The project was conducted in cooperation with the Natick U.S. Army Soldier Center. The ability to deploy steerable round parachutes would reduce costs for the U.S. Army, as round canopies are far less expensive to manufacture than other steerable devices such as parafoils.

Twelve test canopies of inflated diameter 8.645 inches were fabricated from both porous and non-porous nylon materials using a newly designed canopy template. Each canopy was constructed with a unique vent area ranging from 2% - 14% in order to determine which produced the optimal glide ratio. A solid structure was designed to hold the canopies open in a wind tunnel flow. High velocities in the wind tunnel caused vibrations of the solid structure and test setup, therefore testing was restricted to a low freestream velocity of 6.1 m/s. At this velocity, the Reynolds Number based on inflated parachute diameter was 9.1×10^{4}. When compared with studies of air flow over a flat disk which is similar to the flow over a round parachute canopy, this Reynolds Number falls within a range of constant drag coefficient. Therefore it was assumed that the results gathered from the model canopies could be applied to larger-scale round canopies.

The lift and drag on each canopy was measured using a six-axis transducer. It was found that the drag coefficient remained relatively constant as the vent area increased within the range tested. The lift coefficient continually grew as the vent area increased. Using these results, the glide ratio was calculated as lift divided by drag. The glide ratio was found to vary between values of 0.031 at the lowest vent areas and 0.321 at the highest vent areas.

The results show that as vent area increased in both the porous and non-porous canopies, the lift coefficient and glide ratio also increased. It was expected that the data would show an optimal vent area which would create the largest glide ratio at the testing velocity. It is likely that this discrepancy is due to the angle at which the airflow is entering the parachute canopy. When a parachute glides through the air, it has a horizontal component of velocity created by the airflow moving through the vents. In the test setup, the airflow was directly perpendicular to the face of the canopy, therefore decreasing the amount of flow moving through the vents. By orientating the canopy at an angle to the freestream flow in future work, values of the lift coefficients and glide ratios may increase, and an optimal vent area may be identified.

Acknowledgments

The authors would like to thank Professor David Olinger, Professor Michael Demetriou, Dr. Kenneth Desabrais and Dr. Calvin Lee for their help and guidance throughout this project. Also, thank you to the Natick Army Soldier Center for funding this research. Special thanks to Professor John Sullivan and Neil Whitehouse for their patience and time helping three LabVIEW and CNC deprived seniors make this project happen. Finally, thank you to all our friends for keeping us sane throughout the entire project.

Table of Contents

Abstract....2
Acknowledgments....4
Table of Contents....5
Table of Figures....6
List of Tables....7
1. Introduction....8
  1.1 Background....8
  1.2 Previous Research on Parachutes....11
  1.3 Project Objectives....17
2. Scale-Model Parachute Design Process....18
  2.1 Final Design....18
  2.2 Model Design Constraints....19
  2.3 Design Options and Alternatives....23
    2.3.1 Canopy and Template....23
    2.3.2 Frame....25
    2.3.3 Supports....29
  2.4 Scaling of Parachute Model....31
  2.5 Final Scale Model vs. Full Scale Parachute....33
3. Construction....35
  3.1 Support Structure....35
  3.2 Canopy Construction....39
4. Testing Procedure....43
  4.1 Wind Tunnel and Equipment....43
  4.2 Dynamometer....49
    4.2.1 Calibration....49
    4.2.2 LabVIEW Data Acquisition....51
  4.3 Six-Axis Transducer....52
    4.3.1 Setup....52
    4.3.1 Calibration and Alignment....54
    4.3.2 Software....57
  4.4 Velocity Calibration....59
5. Results....60
6. Conclusions....65
7. Recommendations....66
References....67
Appendix A....69
Appendix B....72

Table of Figures

Figure 1: Hoerner's Wind Tunnel Estimations (from Hoerner, 1958) 11
Figure 2: Hoerner's Experiment: Drag of a parachute canopy in presence of a large "load" 12
Figure 3: Balooning of the DEDAL personal troop parachute 13
Figure 4: Vortex shedding over a round canopy (from Desabrais 2002) 15
Figure 5: Cluster of Two Round Canopies 16
Figure 6: Glide Ratio of Clustered Round Canopies 16
Figure 7: Final design for support structure 18
Figure 8: Typical vent geometry for canopies 24
Figure 9: Canopy Template in Pro-E 25
Figure 10: Hooks holding canopy to frame 28
Figure 11: Model of aluminum ring 29
Figure 12: Model of support rod 30
Figure 13: Clamp securing rod to ring connection 36
Figure 14: Rod epoxy connection to ring 37
Figure 15: Setup for bolt attachment 38
Figure 16: Aluminum Stock 39
Figure 17: Aluminum Stock clamped in CNC 40
Figure 18: Final Canopy Template 41
Figure 19: Closed Circuit Wind Tunnel. (From Engineering Laboratory Design [2], 1997) 44
Figure 20: Reynolds Number vs. Drag Coefficient for a flat, circular disk 45
Figure 21: Dynamometer setup in wind tunnel 46
Figure 22: E.L.D Force Dynamometer. (From Engineering Laboratory Design [2], 1997) 47
Figure 23: E.L.D Meter Cabinet 48
Figure 24: Orientation of the dynamometer for drag and lift calibration 49
Figure 25: Drag Calibration Curve 50
Figure 26: Lift Calibration Curves 50
Figure 27: Mean Lift Calibration Curve 51
Figure 28: Setup of the Six-Axis Transducer 52
Figure 29: Drawing of Six-Axis Transducer 53
Figure 30: Transducer attached to frame and sting 53
Figure 31: Screenshot of ATI DAQ F/T Demo Software 54
Figure 32: Directions of the Axis on the Transducer 55
Figure 33: Screenshot of LabVIEW used to collect data 58
Figure 34: Lift and Drag vs. Vent Area for a Porous Canopy 62
Figure 35: Lift and Drag vs. Vent Area for a Non-Porous Canopy 62
Figure 36: Lift and Drag Coefficients vs. Vent Area for a Porous Canopy 63
Figure 37: Lift and Drag Coefficients vs. Vent Area for a Non-Porous Canopy 63
Figure 38: L/D ratio vs. Vent area for Porous and Non-Porous Canopies 64

List of Tables

Table 1: Vent Areas and Dimensions 32
Table 2: X-Direction Calibration of Six Axis Transducer 56
Table 3: Y-Direction Calibration of Six Axis Transducer 56
Table 4: Y-Direction Calibration of Six-Axis Transducer Accounting for Support Structure 57
Table 5: Data Chart of Results 61
Table 6: Drag Calibration 72
Table 7: Lift Calibration 72

1. Introduction

1.1 Background

In the 15th century, when Leonardo DaVinci thought up the idea of a bluff body decelerator that would allow humans to glide like birds, human flight was an unrealistic dream. He was never to see his vision of a parachute put to use, however some have called him the "father of flight" (Carrington, 2000). Today, human flight is an integral part of our everyday lives. It is no wonder then that parachutes have evolved from DaVinci's vision of a clunky and uncontrollable parachute, to the sleek chutes we are familiar with today.

Parachutes are used today for military applications, flight safety systems, and cargo insertion to otherwise unavailable locations. Unlike the "ram-air" parachutes which are used by skydivers, round parachute canopies are larger and less easily controlled (Poynter, 2000). Round parachute canopies have been used to distribute aide to victims of natural disasters and war, insert troops into remote locations, and in the recovery system of the solid rocket boosters for the NASA space shuttle.

Maneuverable parachutes refer to chutes that can glide and turn thereby provide the ability to land on a target or specified location. The first recorded attempt to create a maneuverable parachute was by the Frenchman, Lateur in 1856. He was killed while testing his own design. After Lateur came an American, DeGraff in 1887. Unfortunately, DeGraff shared Lateur's fate. It wasn't until 1929 when E. I. Hoffman developed the Hoffman triangle parachute that a maneuverable parachute was successfully tested. Hoffman was chief of the U.S. Army Parachute Test Group at McCook Field, Ohio. As part of his design, Hoffman placed steering lines on the canopy of the chute which could be pulled by the soldier while in

descent. This would then deform the canopy so that air would be exhausted tangentially, allowing the chute to turn (Knacke, 1992).

During WWII, paratroopers were issued standard T-5 parachutes. These chutes were 28 feet in diameter with a vent hole of 18 inch diameter at the apex. The top hole allowed for airflow through the parachute and therefore release of pressure. The T-5 however had two common problems, the first of which was its controllability. This posed large problems when troopers were attempting to jump in windy or poor weather conditions. Since the chute was difficult to control, soldiers could end up miles off course from their target landing areas. The second problem with the T-5 was its lack of reliability. This issue was mostly resolved with the development of the later T-7 and T-10 parachutes (Cicolello, 1998).

Besides its lack of maneuverability and reliability, the T-5 also gave the jumper a large opening shock. Although soldiers were relieved to feel the shock of the canopy opening, the force on their body would cause cuts and burns. More modern round parachutes such as the T-10C, MC1-1B and MC-1C, create a much smaller opening shock on the jumper, which is often unnoticeable by the paratrooper. Both the MC1-1B and MC-1C are steerable chutes which have material removed from the rear of the canopy to give the chutes a forward thrust of about 8 knots (Cicolello, 1998).

Further development of maneuverable parachutes was encouraged by NASA in the 1960's, when they developed a parachute with the ability to glide toward and land in a pre-selected landing area on the moon. Other requirements given by NASA were that the parachute had to have the capability to avoid such ground obstacles as roads and high power lines as well as land in all types of weather. These requirements lead to the development of various types of maneuverable chutes including the Rogallo wing, or parawing. Today, sport

jumpers most commonly use parafoil parachutes which were invented by D. Jalbert, of the Space Recover Research Center Inc. The parafoil is one of the most easily maneuverable parachutes ever created (Knacke, 1992).

The design of a parafoil is far more complex than that of a round canopy. The parafoil canopy is generally a rectangular shape made up of flexible ribs which are spaced equidistant along the width of the canopy. The ribs form air flow channels where the entering air will maintain the shape of the parafoil (Crowell, 1998).

While round parachutes have the disadvantage of lack of maneuverability, they have an advantage over modern parafoils: round canopies are far less expensive to manufacture. For this reason, there has been great interest in finding a way to allow a round canopy to have glide capabilities and steering. One method which has been investigated by the United States Army is the removal of material from the canopy to create vents. The location, size, opening and closing of these vents will allow a solider to control the descent of the parachute. The use of large, controllable, round canopies will also allow the military to drop cargo from high altitudes, allowing the aircraft to be less vulnerable to fire from the ground (Lee & Buckley, 2004).

Round canopies are ideal for large cargo insertion or safety systems for large aircrafts because of the drag they create. A nearly round shape produces a large drag coefficient when compared with various other shapes when tested in a wind tunnel (Hoerner, 1958). This means that round canopies, either singular or in groupings of 2-3, will be able to descend at a slower rate while carrying heavier cargo than a parafoil. For example, Cirrus has created a parachute safety system for their private, small engine planes. This single, round canopy

system allows the plane to descend slowly enough that the pilot and passengers can land safely, even if the engine were to malfunction in mid-air (Barrett, 2003).

1.2 Previous Research on Parachutes

Hoerner estimated the coefficient of drag on parachute canopies by placing various 3-dimensional objects in a wind tunnel flow. The frontal area of each of the objects represented a stage of opening of a round canopy. He estimated that a fully inflated canopy, with a frontal area to the flow approximated by a circle, created the largest coefficient of drag. Hoerner's estimations can be seen in Figure 1 below (Hoerner, 1958).

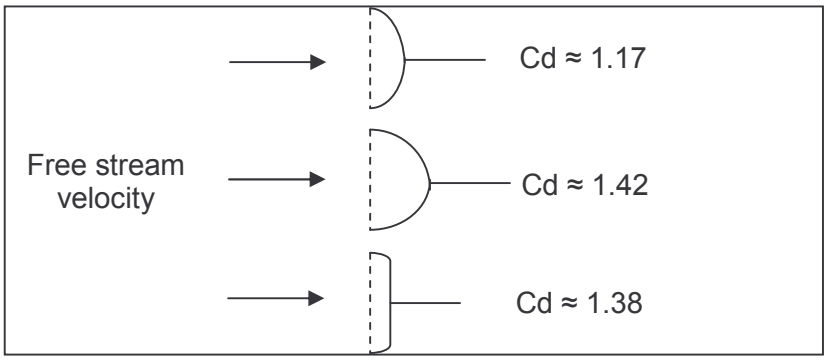

Figure 1: Hoerner's Wind Tunnel Estimations (from Hoerner, 1958)

Hoerner also summarized the effects on drag forces when placing a load on a canopy. He estimated that the wake created by the load would reduce the drag coefficient on the canopy by approximately 22%, assuming that the diameter of the load was 1/3 the size of the canopy itself. This calculation however does not take into account the mass of the load, nor the length of the suspension lines. A recreation of Hoerner's sketches of this experiment can be seen in Figure 2 (Hoerner, 1958).

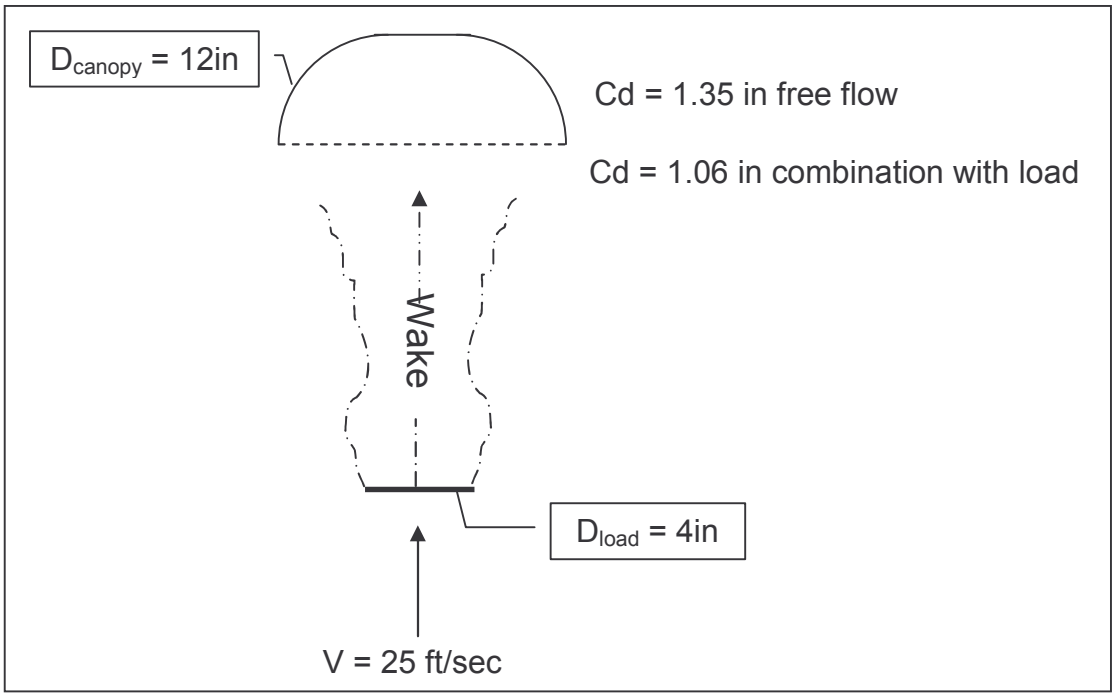

Figure 2: Hoerner's Experiment: Drag of a parachute canopy in presence of a large "load"

Full scale canopies are constructed by sewing individual panels together to form their circular shape. These panels are called “gores” (Desabrais, 2002). Canopies are connected to suspension lines at the end of each gore, allowing the canopy to “balloon.” Ballooning is the spreading of the bottom of the canopy to form semi-circular shapes spaced around the circular base. An example of canopy ballooning can be seen in Figure 3.

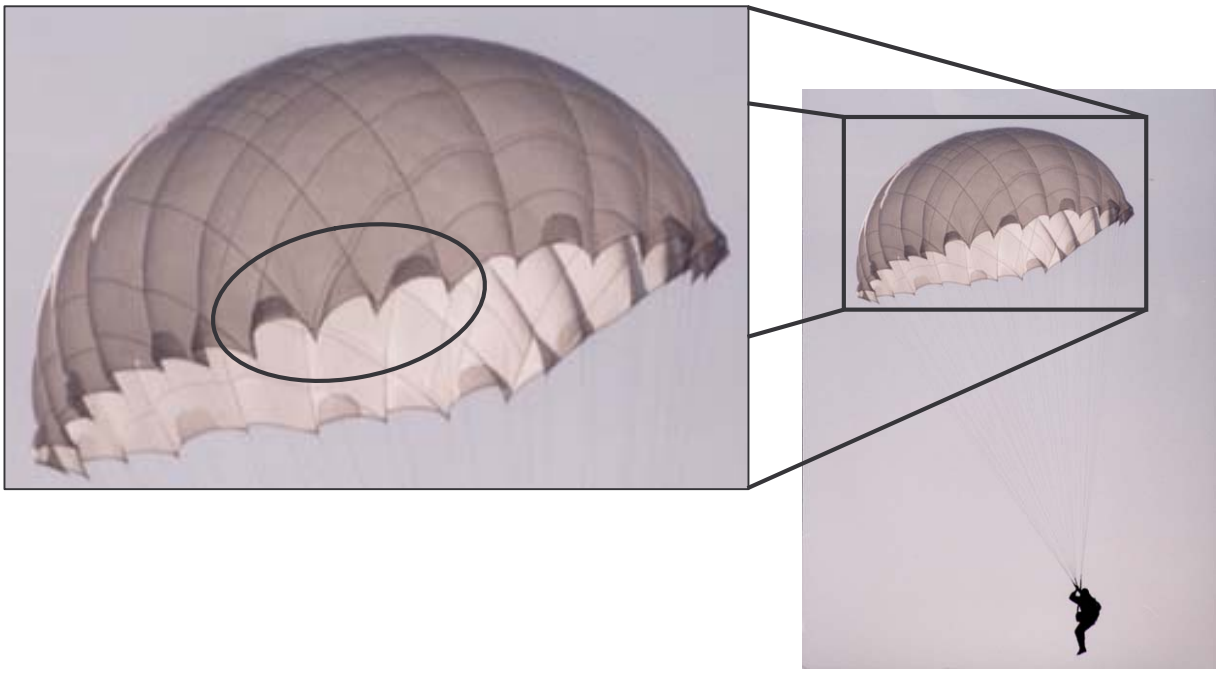

Figure 3: Balooning of the DEDAL personal troop parachute

While in descent, a round canopy will also experience some "breathing." Breathing effects are created by the steady movement of the canopy in and out as it descends. When compared to the effects of lift and drag on the descending parachute, the effects of breathing on the canopy are minute.

Parachute canopies can be manufactured from porous or non-porous materials. The porosity of the canopy affects the parachute drag, stability and opening forces. As the porosity of the material increases, the drag, stability and opening forces all decrease. While a decrease in opening forces is desirable, a decrease in drag forces and stability is not (Knacke, 1992).

Historically, experimental data obtained by placing a sphere in a fluid flow has been used to estimate the forces on a round parachute canopy. A sphere was chosen because the characteristic area, or area seen by the fluid flow, of a sphere is very similar to that of a round canopy. Recently however, it has been found that there are two problems, canopy flexibility

and porosity are not accounted for in wind-tunnel testing of a sphere. The flexibility of the canopy fabric allows for noticeable variations in the geometry of the canopy. These variations occur not just while the canopy is opening, but also once the canopy has become fully inflated and is in steady decent. Experimental data obtained from sphere testing does not account for this variable because the sphere has a fixed geometry. Secondly, when testing a porous fabric canopy, there is a velocity flow which is allowed to pass through the canopy itself. This flow can accumulate to a few percent of the free stream velocity which is being tested. The flow through the canopy will cause discrepancies between data obtained from using an impermeable sphere and data obtained from testing a porous canopy (Johari, 2005).

Recently, tests have been run on the opening effects of a round parachute canopy. These experiments utilized a water tunnel and a scale model canopy with 24 tie lines evenly spaced around its circumference. One result of this testing was the realization that vortex shedding around the parachute canopy begins when the canopy is approximately 68% at its fully inflated diameter. The figure below shows the vortex shedding of the water stream as it flows past the round canopy. As the canopy reaches its maximum diameter, the shedding becomes less symmetric (Desabrais, 2002).

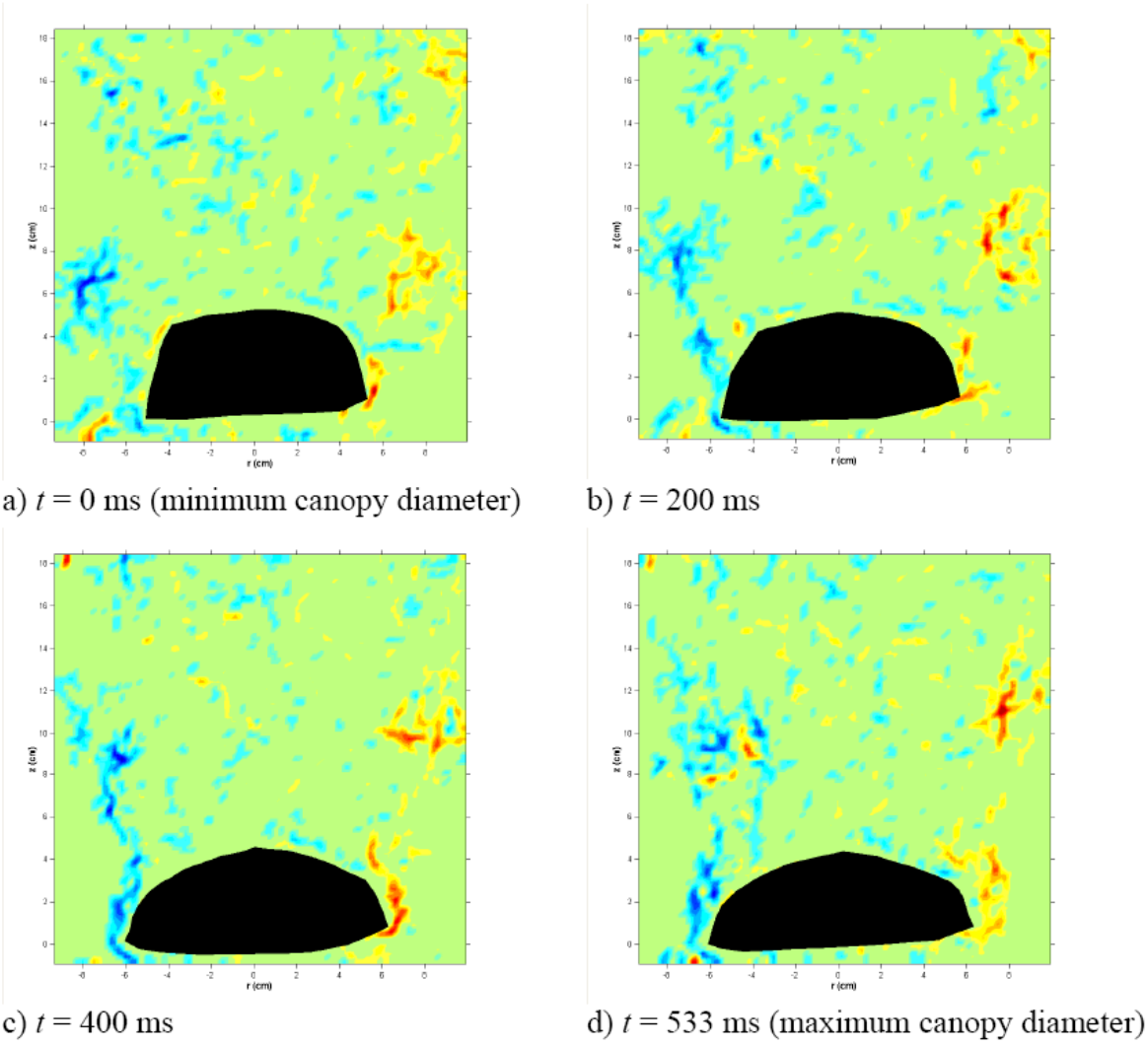

Figure 4: Vortex shedding over a round canopy (from Desabrais 2002)

Tests have also been done to measure the glide ratio of a cluster of round canopies. This was done by dropping a cluster of two one-quarter scale G12 canopies from approximately 300 meters. This cluster can be seen in Figure 5.

Figure 5: Cluster of Two Round Canopies

The measurements of the glide ratio on the two canopies as the cluster descends can be seen be seen below.

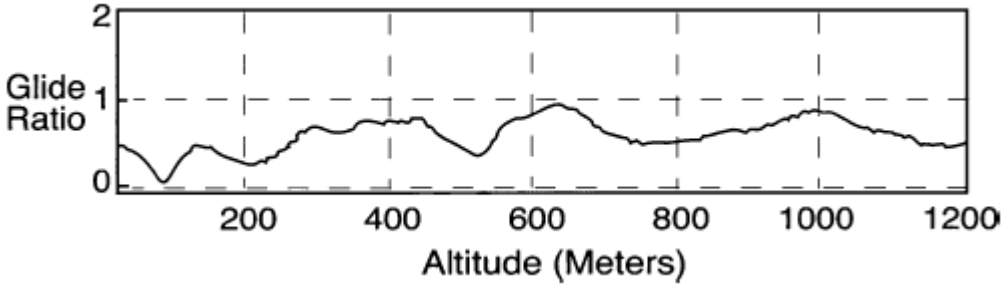

Figure 6: Glide Ratio of Clustered Round Canopies

1.3 Project Objectives

Our objective for this project was to study the effects of canopy vents on the performance of round parachutes. Scale-model wind tunnel testing of round parachutes of similar structure and material to a full scale chute was conducted for both porous and non-porous materials.

Since multiple vent sizes and placements were tested, it was necessary to manufacture multiple canopies, each with varying vent sizes. The lift and drag forces and coefficients on each of the canopies were measured using a closed-circuit wind tunnel. The glide ratio was then determined for each variation of size, vent placement, and material. A template was designed and manufactured in order to exactly replicate the format of each canopy. This template was not only used to create each of the canopies, but to vary the vent sizes while maintaining a constant geometry and symmetry of each vent.

Two canopy materials were tested, one a 1.1oz/sq. yd porous nylon commonly used for cargo insertion, and one non-porous material. Six canopies were made of each material, each one with vents covering a different percentage of the total flat area of the nylon. Vent areas ranging from 2-10% were cut from the porous material, while the non-porous vents areas ranged between 6-14%. One control canopy without vents was created from each material as well.

2. Scale-Model Parachute Design Process

2.1 Final Design

The final design for the canopy support structure is presented in Figure 7.

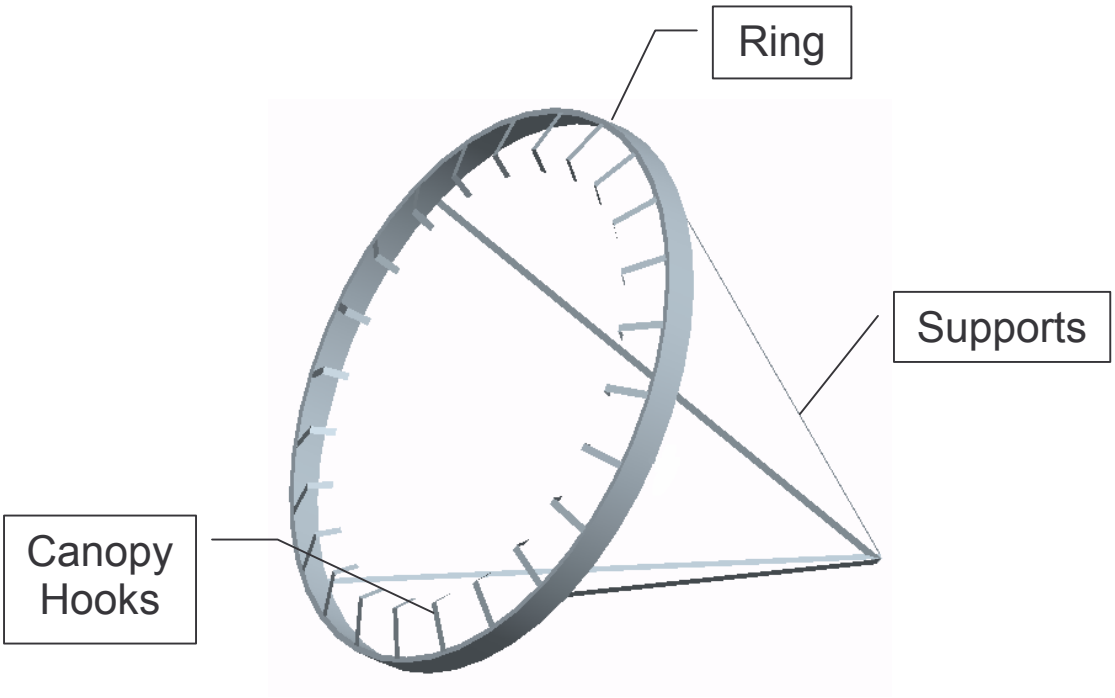

Figure 7: Final design for support structure

A summary of the process used to design the canopy support structure including design alternatives and model constraints can be found in the following sections.

2.2 Model Design Constraints

WPI's closed circuit wind tunnel was used because closed circuit wind tunnels provide a more uniform flow throughout the test area providing better data (Knacke 2002). The size of the wind tunnel test section is 2'x 2' and the scale model must attach to a force balance that protrudes into the wind tunnel vertically. The force balance will record the lift and drag of our vented parachutes. This is just one of the many constraints we had to keep in mind when designing our scale-model parachute.

One design constraint that was considered was possible flow-induced vibration of the canopy support structure. When a forcing frequency present in the flow matches the natural frequency of the object large amplitude vibrations can result.. These vibrations would effect measurements of lift and drag in the parachute experiments. The Strouhal number is a dimensionless number that describes the vortex shedding that occurs behind parachutes placed in a free stream flow. The Strouhal number can be found by using:

$$St = \frac{fD_p}{V_\infty} \qquad (1)$$

Where St is the Strouhal number, f is the shedding frequency, V_∞ is the free steam velocity and D_p is the projected diameter. A Strouhal number of 0.55 for parachute canopies has been observed by Ken Desabrais (Desabrais 2002). If the frequency, f, matches the natural frequencies of our structure then we would encounter the vibrations. Solving for f gives us:

$$f = \frac{Vortices}{Sec} = \frac{0.55(V_\infty)}{D_p} \qquad (2)$$

At velocities of 10, 18 and 25m/s we found the shedding frequencies to be 25.41, 45.74, 63.52 Hz respectively. Next we need to compare these numbers to the natural frequency.

To calculate the natural frequencies we consdiered each part separately. The equation for the ring is:

$$f_i = \left[\frac{\left(1+2i^2\right)^{0.5}}{2\pi r}\right]\left(\frac{E}{\mu}\right)^{0.5} \quad (3)$$

Where i =1,2,3... and denotes the mode, r is the radius of the ring, E is the elastic modulus and μ is the mass density (Blevins 1979). The frequencies were 2989 and 4726 Hz for modes 1 and 2 respectively, which are much larger than the shedding frequencies found earlier.

The supports have a natural frequency defined by:

$$f_i = \left[\frac{{\lambda_i}^2}{2\pi L^2}\right]\left(\frac{EI}{m}\right)^{0.5} \quad (4) \qquad \text{where} \quad \lambda_i = \left(2i+1\right)\frac{\pi}{2},$$

L is the length, I is the moment of inertia and m is the mass per unit length (Blevins 1979). For modes 1, 2 and 3 the natural frequencies were 88.2, 243.3 and 476.9 Hz. Mode 1 of the supports is fairly close to the 25m/s shedding frequency however, later in this paper, it will be discussed that a freestream velocity of 25m/s will not be used in the testing.

Another constraint was wind tunnel blockage effects. When any object is placed in a wind tunnel flow, it creates a blockage effect due to the constraining effect of the wind tunnel walls that interfere with flow over the object. The blockage ratio is found using:

$$b = \frac{A_p}{A_{wt}} = \frac{\pi\left(.355\right)_p^{\ 2}}{\left(2\right)\left(2\right)} = 9.9\% \quad (5)$$

Where b is the blockage ratio, A_p is the projected area of the parachute and A_{wt} is the cross-sectional area of the wind tunnel. Our canopy had an inflated diameter of 0.71 ft. This diameter was found by using a blockage ratio of <10%. Thus, we chose a blockage percent of 9.9% and solved for the diameter. When the blockage ratio is too large, the diverting

streamlines will cause a large enough disturbance in the flow to affect lift and drag data. (Day 2006)

Obtaining accurate readings from the force balance was an additional constraint. Day et al. (2006) found that the range of forces the dynamometer can accurately read is 0.35 – 7lbf. We chose a rigid support for our canopies. The support was made of metal and thus did not have a negligible weight to it. The weight caused a downward force on the dynamometer which had to be accounted. The system was oriented so the vents in the canopy would be towards the bottom and therefore produce an upward lift force to counteract the weight of the support. However, as discussed in Section 4.3, our second force balance required us to orient the vents so they were lined up with the side wall of the wind tunnel

The horizontal force, or drag force also could not exceed 7 lbf. This constraint however was interrelated with other constraints because the projected area of the parachute and the speed of the wind tunnel are what dictated the maximum drag forces. The projected area of the canopy was bound by the blockage effect. We could not make the area any larger because the blockage effects would be too high.

Higher wind tunnel velocities create a larger force. This can be seen by first considering Lift and Drag forces. These forces are caused by pressure differentials resulting in a net non-zero force and hence producing lift and/or drag. So the Lift and Drag forces are proportional to the pressure and the air in the wind tunnel be taken as an incompressible fluid because of the low speed. Bernoulli's principle is given by,

$$\frac{V^2}{2} + \frac{P}{\rho} = K \quad (6) \qquad \text{where } K \text{ is a constant.}$$

Lift and drag are non-dimensionalized using lift and drag coefficients given by:

$$C_L = \frac{L}{\frac{1}{2}\rho V^2 A} \quad (7) \qquad C_D = \frac{D}{\frac{1}{2}\rho V^2 A} \quad (8)$$

Where ρ is air density, V is the wind tunnel velocity and A is the area of the parachute.

These equations allow the lift and drag to be viewed as dimensionless numbers and also show that V^2 is proportional to Lift and Drag.

2.3 Design Options and Alternatives

2.3.1 Canopy and Template

The goal of this project is to test different vent sizes in non-rigid round canopies. We were given two different materials to test by our advisors from the Natick Army Soldiers Center. We received 1.1 ounce per square yard porous nylon and a non-porous nylon to use in our testing. The canopies will be cut out of large pieces of fabric with a soldering iron so that we will get clean cuts and there will be no fraying of the material. Real parachutes are made by sewing wedge shaped sections called gores together to make the canopy. However for the small scale models we have, it was not practical to sew gores together to make each of the 10 canopies. By using one solid piece of material we can ensure similarity between models while sacrificing very little. In order to ensure that each of these canopies will be as similar to each other as possible we designed a template to be used when cutting out each of the canopies.

We used CNC machines available at WPI to precisely cut out a flat, ½ of an inch thick, circular, aluminum disk. Aluminum was chosen as the material because it is relatively easy to machine and since the soldering iron used to cut the canopy would not change the shape of template. It was decided that the flat diameter of the canopies would be 1 foot and the flat plate was designed to have exactly that diameter. To replicate full scale parachutes as closely as possible we decided that the canopy would be attached to the frame at 24 points. This is close to the number of lines full scale parachute have and will help to reduce the magnitude of the canopy ballooning. The canopy will be attached to the frame with hooks, as described below. To ensure the holes for the hooks are in exactly the correct spots there will be holes drilled into the template with a diameter of .125 inches placing their centers are .125 inches

from the outer edge of the plate. These holes are spaced at 15 degree increments. The diameters are sized so that the diameter of the soldering iron fits in the holes. This makes the actual hole in the canopy made by the soldering iron exactly in the center of each hole cut in the template. In addition to these holes there will be a 1 inch diameter hole in the center of the template to correspond to the round vent that is in the center of most round parachutes. We were not able to scale this center vent exactly to a real parachute because we believed it would have been to large relative to the size of the canopy. After discussion with our advisors we settled on the size of 1 inch diameter. The figure below shows a typical vent geometry for the model canopies.

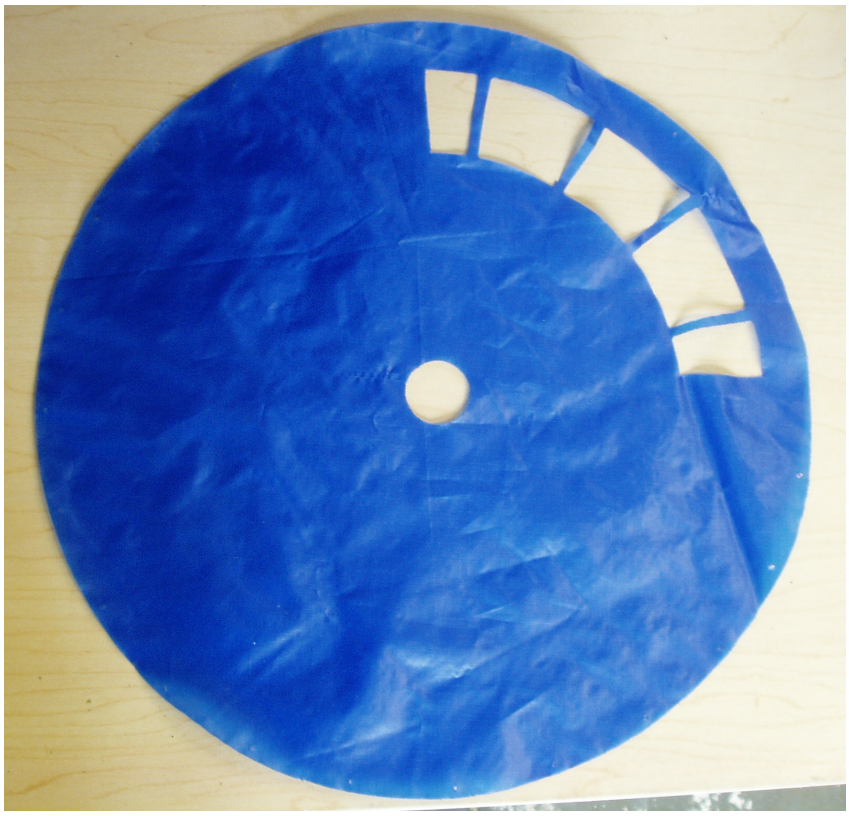

Figure 8: Typical vent geometry for canopies

The vent sizes in all of the canopies are wedged shaped and have identical heights. The shape of the largest vent size to be tested was milled out of the plate symmetric to a hook hole. The exact dimensions of the vents are shown later in this report. In order to be able to cut the intermediate vent sizes we designed an insert out of wood with a metal face. The insert is able to fit into a vent to enable us to cut out a vent size that is half the size of the cut in the template. This template gives us an accurate, consistent, and easily repeatable way to cut out vent sizes in our canopies. The template can be seen in Figure 9.

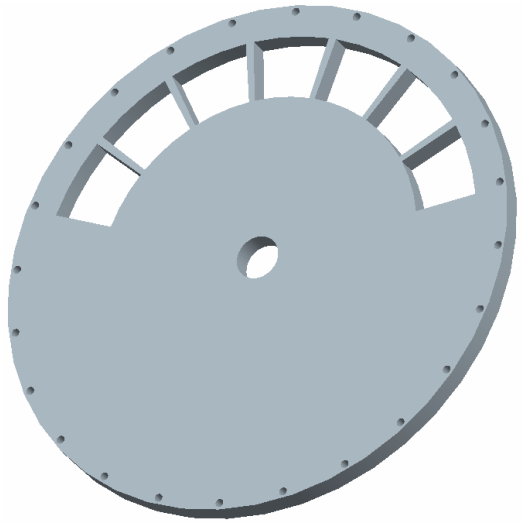

Figure 9: Canopy Template in Pro-E

2.3.2 Frame

The goal of the frame was to ensure that the vibration of the canopy was kept to a minimum during testing in the wind tunnel. To do this it was decided to construct a rigid frame that would hold the canopy in a fully inflated state, which was determined to be 8.54 inches in diameter.

The first decision to be made was where the frame would be located with respect to the canopy. Our options were to have the frame far outside of the canopy, the canopy connected to the inner sides or outer sides of the circular frame. Having a frame far outside the diameter of the canopy solved the issue of flow interference. However issues arose with connection of the canopy to the frame and the measuring of forces. In order to connect the canopy there would need to be thin stings running across the diameter of the frame. This webbing allows breathing to occur in the model, which is closer to real life, but would also allow for vibrations and excessive movement. It would also be near impossible to take force measurements with the force balance due to the lack of rigid connections from the canopy to the frame. Due to all these disadvantages this method was discarded.

The two options of having the canopy attached to the outside or the inside of the ring were thoroughly debated and the conclusions are as follows. Having the canopy attached to the outside of the frame allowed there to be no possibility of inference between the frame and any ballooning that might occur. However this left the frame directly in the airflow that would be heading into the canopy and into our vents. Attaching the canopy to the inside of the frame posed the exact opposite dilemmas. Because the canopy was attached to the inside of the frame, the frame would not disturb the airflow going into the canopy but it had the possibility of interfering with any ballooning of the canopy. However, by redesigning the hooks that would attach the canopy to the frame so that the canopy was lifted a little above the frame we were able to overcome the problem of interference in ballooning. This led to the adoption of the canopy attaching to the inner side of the frame as our final design as shown in Figure 15. However, because we are using a rigid frame to hold the canopy, breathing is not

able to occur. It was decided that the loss of breathing was not as important as being able to eliminate the canopy vibrations.

We decided that we were going to use hooks to attach the canopy to the frame so that each of the canopies can be attached and removed with relative ease. Because of this it is possible to use the same frame in every test and therefore eliminating a possible variable in testing. The first option we investigated was to use small aluminum strips which would be bent at and angle and would be spot welded directly to the frame. These strips would be cheap and easy to make and easily replaceable should one get damaged and destroyed. However the peak of these strips would be touching the frame and therefore may cause bunching of the canopy material. Also, as mentioned above, when attached to the inner side of the frame the canopy material would not be able to balloon due to contact with the frame. The second option considered was the use of fishing hooks attached to the frame with epoxy. It was decided that extra long size #14 fishing hooks (with their barbs flattened) would be a good size to attach to the frame. By attaching the hooks half way up the frame it allows the top of them to be sufficiently high enough to allow the canopy to be above frame enabling the canopy to balloon freely. To compensate for the hooks being inside the frame while keeping the inflated canopy size at 8.54 inches the diameter of the frame was set to 8.64 inches. The next step was to design and manufacture this frame.

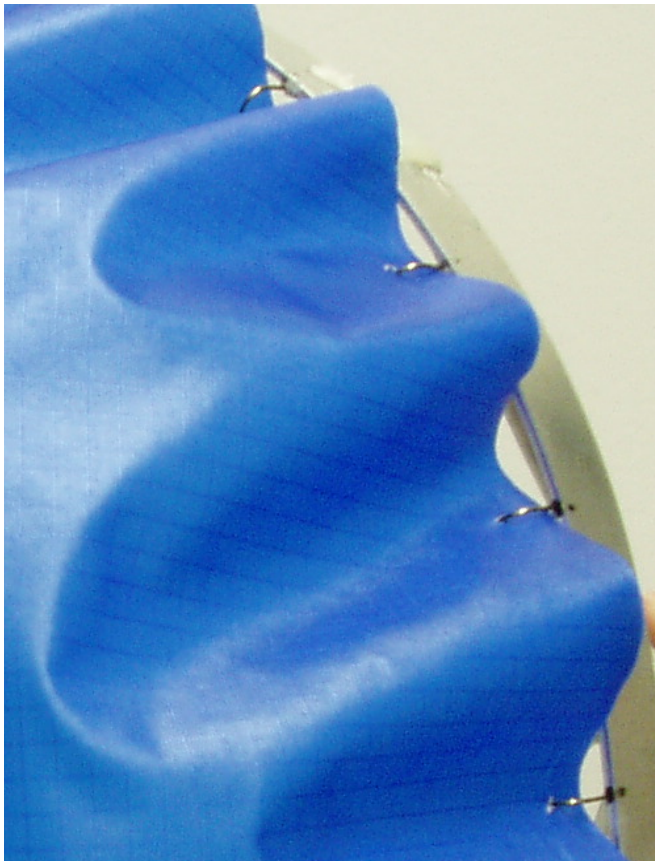

Figure 10: Hooks holding canopy to frame

One of the first options discussed was a machined circular aluminum ring. The aluminum would be manufactured by the CNC machines in the facilities at WPI. The advantages of this steel frame are its exact dimensions and rigidity. Because it would have been fabricated by CNC machine the diameter and thickness of the ring would be precisely machined. The properties of aluminum would have also ensured that ring would have stayed rigid during testing. However the CNC machined frame had a number of disadvantages that led to its dismissal as a design option. The machining of such a large piece of metal would have taken a large amount of time and led to a large amount of waste metal.

The option that we decided on as our final design was a ring that was made of a piece of aluminum sheet metal. The sheet metal would be orientated so that the thinnest part would

be facing into the airflow. This allows the frame to have minimal interaction with the flow. In order to ensure rigidity and to allow ample space to attach the hooks it was decided that the sheet metal would be ½ inch in length in the flow direction. We found that a .05 inch thick aluminum sheet metal was rigid enough to be used as our frame. A model of the aluminum frame can be seen below.

Figure 11: Model of aluminum ring

2.3.3 Supports

It was also necessary to determine how we were going to connect the frame to the dynamometer. We determined that we needed 4 rigid, thin supports that connected from the frame to the dynamometer. Because the canopy was already attached to the frame at 24 points we determined that it was unnecessary to have a large number of supports that would interrupt the airflow heading into the canopy. Steel rods of 1/8 inch diameter were used for the supports. It was determined that the length of each support should be equal to the

diameter of the parachute. This requires that each support be at a 60 degree angle with respect to the frame. Therefore the length of each support would be 8.64 inches long, however we added a half an inch making it 9.14 inches long so we would be able to use that extra half an inch to attach the support to the frame. By grinding the top half inch of the support to make it somewhat flat we make attaching the rod to the frame sturdier and easier. We also bent it in the correct 60 degree angle with respect to the frame so that each of the four supports converges at the same spot. The bent rods are shown in Figure 12.

Figure 12: Model of support rod

In order to attach the supports to the force balance we obtained a bolt that has a quarter inch diameter threading to fit directly into the force balance sting threading. We decided that the simplest and most effective way of attaching the supports to the bolt was to epoxy them directly to the head of the bolt. We used a nut to secure the bolt to the sting to ensure that it would not rotate about the sting axis during testing. This also allows us to secure the supports and frame at any angle we so desire.

2.4 Scaling of Parachute Model

We also needed the ability to test multiple parachutes, each with various vent sizes. Because of the complexity involved in making a parachute with 24 or more flexible rigging lines, we chose a rigid support system with hooks that allowed for a quick interchange of canopies. This system needed to be small enough as to not disturb the flow significantly and also be lightweight as to not create a large moment arm on the force dynamometer. Aluminum was chosen as the primary metal because it is lightweight and easy to machine. The support system was devised of a ring, four supports, ¼" threading and 24 hooks.

Because of the blockage effects, the canopy's inflated diameter was chosen to be 8.52 inches in diameter. The diameters of inflated canopies are roughly 71% of their non-inflated diameter. This results in a total surface area of 113.1 in^2. Once we knew the total area, we had to determine the best vent size and placement. Our liaisons from Natick had recommended we use a baseline average vent area of 6% for non-porous and 10% for porous. Therefore, using a 2% increment, we tested 6, 8, 10, 12 and 14% vent areas for the porous nylon and 2, 4, 6, 8 and 10% vent areas for the non-porous nylon. See Figure 8 for geometry of 8% vent area. The scale model canopy had 24 holes spaced 15 degrees apart for attachment to the support structure. They reached 3/16" from the edge which forced our vents to start at 5.75" from the center of our flat canopy. The vent size was determined using by scaling the vent sizes of a G12 canopy (Lee 2004). We also used curved rectangles as the shape for the vent. The vent was decided to be a quarter length around the circumference of the canopy for the 10% area. Using geometry you have the two following equations:

$$S = r_m \theta_{rad} \quad (9) \qquad wh = A_v \quad (10)$$

Where S is the arc length, r_m is the radial distance to the midline of the vent, θ_{rad} is the angle the vent sweeps across, w is the width of the vent, h is the height of the vent and A_v is the area of the vent. We then equated the arc length S to the width of the vent w, resulting in:

$$w = \left(5.75 - \frac{h}{2}\right)(1.571) \qquad (11) \qquad\qquad wh = 11.31 \qquad (12)$$

Solving these equations simultaneously resulted in a height of 1.43" and a width of 7.91". We then held the height constant for all other vent sizes and varied the length. When this was given to our Natick advisors they recommended two things. First we should move the vents in by 0.5 inches because the original layout did not leave enough material for structural integrity. Secondly we were to leave small strips of material in the vent so that the canopy again had structural integrity. These were incorporated into the model. First we moved the vents closer to the middle and kept the height constant. For our redesign, θ_{RD} now equaled $20°$. We then had to separate each % increment by a thin strip of nylon. We decided to use a thickness of 3/16" at the midpoint of the vent and using the arc length equation above, each strip of nylon resulted in a 2.05 º slice. We added this in between each incremental area. Table 1 shows geometric parameters for the redesigned canopies.

Vent %	2%	4%	6%	8%	10%	12%	14%
Vent area (in^2)	2.26	4.52	6.79	9.05	11.31	13.57	15.83
Height (in)	1.43	1.43	1.43	1.43	1.43	1.43	1.43
Width (in)	1.58	3.16	4.75	6.33	7.91	9.49	11.07
Sweeping Angle (deg)	20	40	60	80	100	120	140
Separation Strip Thickness (deg)	2	2	2	2	2	2	2

Table 1: Vent Areas and Dimensions

2.5 Final Scale Model vs. Full Scale Parachute

In many ways, our scale model parachute mimics the structure and movement of a full-scale parachute. For example, the rigid support has been designed to allow ballooning of the parachute canopy. As seen in practice, full-scale parachutes also have a ballooning movement as they descend. Although the effects of canopy ballooning may be small, they will be accounted for in our measurements of lift and drag.

The Reynolds number of our scale model setup was calculated as 9.126×10^4. A full-scale canopy has a Reynolds number on the order of 10^6. As can be seen in Figure 20, each of these Reynolds numbers fall along an area of constant drag coefficient on a plot of Cd vs. Reynolds number for flow over a flat, circular plate. As this flow is similar to a flow over a round parachute canopy, it is assumed that the drag coefficient will not be greatly affected by testing a canopy of lower Reynolds number.

The vent sizes and locations on our scale model parachute have been determined using the information gathered from full-scale parachutes used by the U.S. Army. This means that their geometries and placements closely mimic those of the larger chutes and hopefully will allow for a similar fluid flow. These scaled vents include the apex hole which has been cut in the top center of each of the scale model canopies.

There are however, some differences between our experimental apparatus and a full-scale parachute, which may cause for errors in measurement. Perhaps the largest difference is the lack of suspension lines. In order to assure that the canopy remains inflated and steady during testing, it was decided best to create a rigid support to hold the canopy in the wind tunnel. Although the lengths of the support bars was set equal to the open diameter of the canopy, similar to the suspension lines in a full-scale chute, the rigid bars will create

disturbances in the flow. These disturbances will certainly have some kind of effect on the lift and drag measurements.

Attached to the rigid supports was an aluminum ring holding the canopy inflated in the flow. Although the flow will be allowed to enter the open canopy mostly undisturbed, the canopy itself will not be allowed to breath. The breathing effect, as discussed earlier, is the movement of the parachute in and out as it descends. Again, restraining the canopy from making this natural movement will likely have an effect on the measurements taken in the wind tunnel.

The final significant variation between the full-scale parachute and the testing device is the lack of gores on the scale-model canopies. Round parachute canopies are created by cutting the nylon into triangularly shaped gores; as the scale model canopies are made from a single piece of nylon, they will not exactly mimic the movements of a full-scale chute.

Overall it will be assumed that these differences in structure and movement between the experimental apparatus and a full-scale parachute will have little effect on the measurements of lift and drag taken in the wind tunnel.

3. Construction

3.1 Support Structure

We obtained an aluminum sheet metal with a thickness of .025 inches we then marked it with the proper dimensions of 27.15 inches long and ½ inches high. Using a jump shear located on campus we were able to make a precise clean cut. However, after some testing on the .025 inch thick aluminum, it was determined that it was far too flexible for our project. We then found .05 inch thick aluminum sheet metal and cut it to the proper dimensions. The twofold increase in thickness gave the ring the rigidity that we required. Before we formed the cut sheet metal into a ring we marked where the hooks and rods connected with permanent marker. A hook was to be placed every 1.13 inches while the rods were to be placed at 6.79 inch intervals. We gave the strip to the Higgins Laboratories' machine shop head Neil Whitehouse for bending and welding. He used a sheet metal roller to bend it to a perfect circle then used TIG (tungsten inert gas) welding to get the aluminum ring to hold its shape. TIG welding is one of the few reliable, conventional methods to weld aluminum. The next step was to create the rods that would connect the ring to the bolt.

We found .125 inch diameter steel rods in the machine shop supply room. Using a large table clamp in the machine shop we bent the rods using our hands. To verify the angle we used a protractor to make sure we had bent them 30 degrees. At the center of each angle we measured .5 inches in one direction and 8.65 inches in the other direction and made a mark at each point. Then using large wire cutters we cut the steel rods to their proper dimensions. The long steel rod was marked at 9.14 inches long intervals and then cut with large wire cutters at those intervals. With the four supports completed we obtained a ¼ inch diameter, 3 inch long bolt to attach the rods to the force balance. Using a small diameter file we were

able to put groves in the bolt at 90 degree angles to allow the rods a place to sit into. With all the individual parts of the support structure manufactured the only step left was assembly.

Due to the fact that it is difficult to weld steel to aluminum we had to attach all of our parts using Devcon 5 minute gel epoxy. Due to the full day of setting time needed for the epoxy we attached the rods to the ring at a rate of one per day. After scratching the surface of the ring the marks we had placed on the ring earlier with a rock to help the epoxy attach to the aluminum, we lined up the ½ inch long end of the rod with the mark and put a small amount of epoxy on. We then used a small clamp to hold the rod in place overnight as shown below.

Figure 13: Clamp securing rod to ring connection

Figure 14: Rod epoxy connection to ring

Twenty four hours later we would put additional epoxy on the connection while attaching the next rod to the ring as shown in Figure 14.

After all four rods had been attached to the ring we had to connect the bolt to the rods. The plane of the bolt had to go exactly perpendicular to the plane of the ring to ensure that the canopy would be perpendicular to the flow in the wind tunnel. In order to ensure that we attached the bolt correctly we build a frame to hold the bolt out of wood. The ring is positioned laying flat on a table with the supports facing up with the bolt above inside the support. The bolt is then maneuvered in-between the rods and epoxy is added to connect the bolt and rods together, as seen below. Once the epoxy had set we were able to move on to the last part, the attachment of the hooks to the ring. Using the previously marked spots on the ring we attached each fishing hook with small amounts of epoxy. The tip of each hook was

positioned so it was at the same height as the top of the ring. This allows the canopy to be above the ring.

Figure 15: Setup for bolt attachment

3.2 Canopy Construction

A CNC machine was used to fabricate the template. This allowed us to program the part into Pro-Engineer, a CAD software package. The part as seen in Figure 9, requires many precision cuts for the template to be manufactured exactly as designed. CNC machines can handle the precision cuts with ease and once we had the final design; it was time to put the Pro-E file into GibbsCAM. GibbsCAM is another useful software program designed to import CAD files and turn them into the machining code that the CNC machines need to run. This was done with much help by the Higgins machine shop. Once programmed into GibbsCAM the part was cut out from Aluminum stock show here in Figure 16.

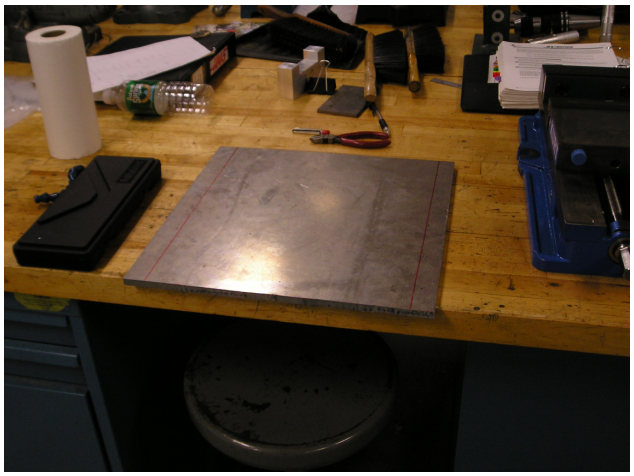

Figure 16: Aluminum Stock

The aluminum stock is 0.4" thick and 16"x 16" across. The aluminum piece was then placed into one of WPI's Haas CNC machines. The work coordinate center was set to be the exact center of the aluminum stock to allow plenty of space along the sides for clamps as you can see in Figure 17. The reason for this piece was so that it can be placed on top of a piece of nylon and the parachute can be cut out of the nylon by using a soldering iron.

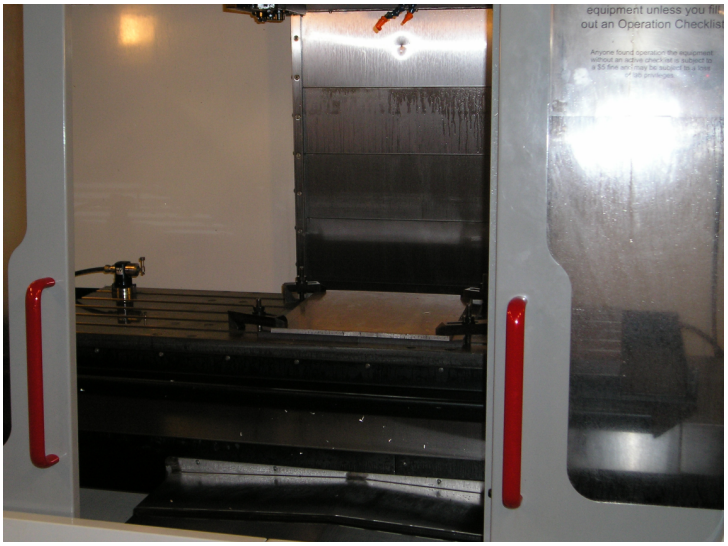

Figure 17: Aluminum Stock clamped in CNC

The soldering iron has a tip diameter of 1/8", but we manufactured 3/16" holes into the template to allow for some tolerance. We also kept 1/16" of material between the edge of the entire template and the closest edge of soldering iron holes. An attempt to scale the size of the center hole from a larger G12 canopy failed. This would result in a hole that was far too large for our small parachute. In a meeting with our Natick and WPI advisors we all agreed on a one inch diameter center hole. This should allow for full inflation without losing too much flow through the vent holes. The final product can be seen below.

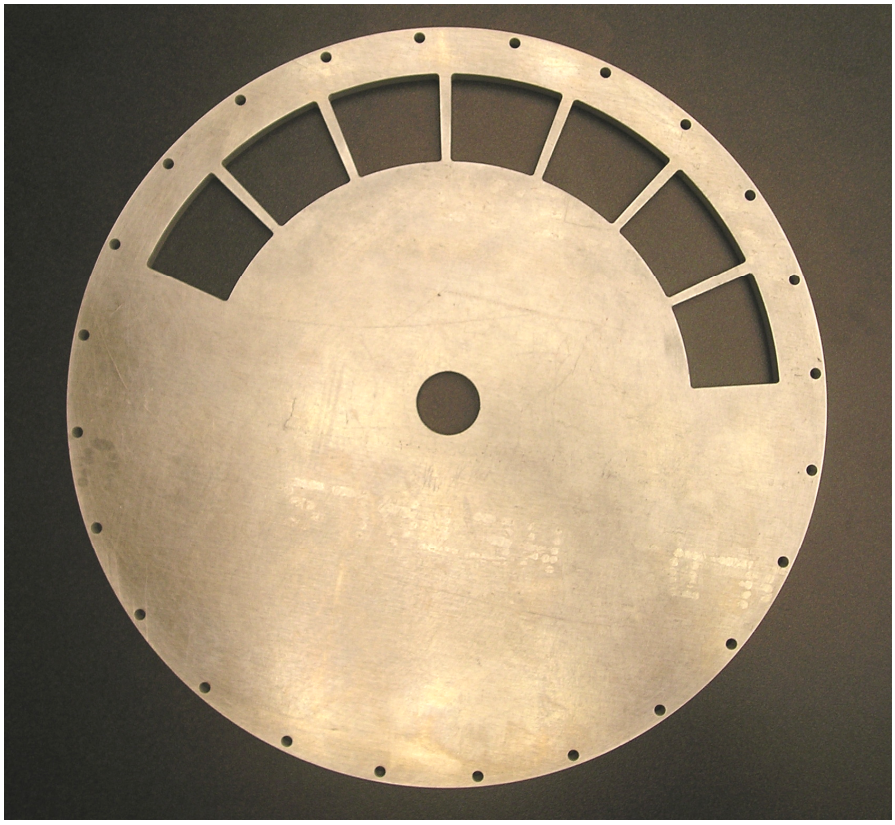

Figure 18: Final Canopy Template

We also designed this part to be symmetric and as you can see the center vent on our template lines up perfectly with one of the 24 edge holes. This means that we needed a small insert that swept out 10º and had a height of 1.43 inches. Since the machined part can not have exactly square corners because of the rounded bit, we decided to make the insert out of wood because it was easy to sand the corners down to fit into the template. For example, to make a 14% vent area one would simply cut out every available vent hole on the template. However, to make a 12% differential you must leave out one 20º hole. You can not simply cut 6 of the 7 holes out and leave the last one because the vent area would no longer be symmetric with the edge holes. This problem is solved by using our insert. You simply place the insert into the end vent areas on either side and only cut out half of each hole. This gives you your necessary 12% vent area. For 10% you leave the end vent areas on either side alone

and do not cut them out. And likewise for 8% you would simply place the insert into the second hole from the end on either side and only cut half of those while leaving the end holes alone too.

4. Testing Procedure

4.1 Wind Tunnel and Equipment

The wind tunnel which is being used for testing is a 24" recirculating, closed-circuit wind tunnel manufactured by Engineering Laboratory Design Inc. This closed-return wind tunnel was chosen for the testing primarily because of it's 2 x 2 x 8 ft. test section. However, there are other advantages of using a closed-circuit wind tunnel vs. an open-circuit tunnel. When the tunnel is closed, the quality of the flow can be more easily controlled. Also, there is lower energy required for a given test section and velocity, as well as less noise than an open-circuit tunnel (Rae, 1984).

The velocity in the test section is controlled by adjusting the RPM of the fan shaft. The velocity range in which the tunnel may operate is 3.05 m/s to 54.9 m/s. Twelve clamps secure the test section which may be accessed by removing either the ceiling or the floor (E.L.D., 1998). Below is a diagram of the wind tunnel which will be utilized for our measurements (E.L.D., 1998).

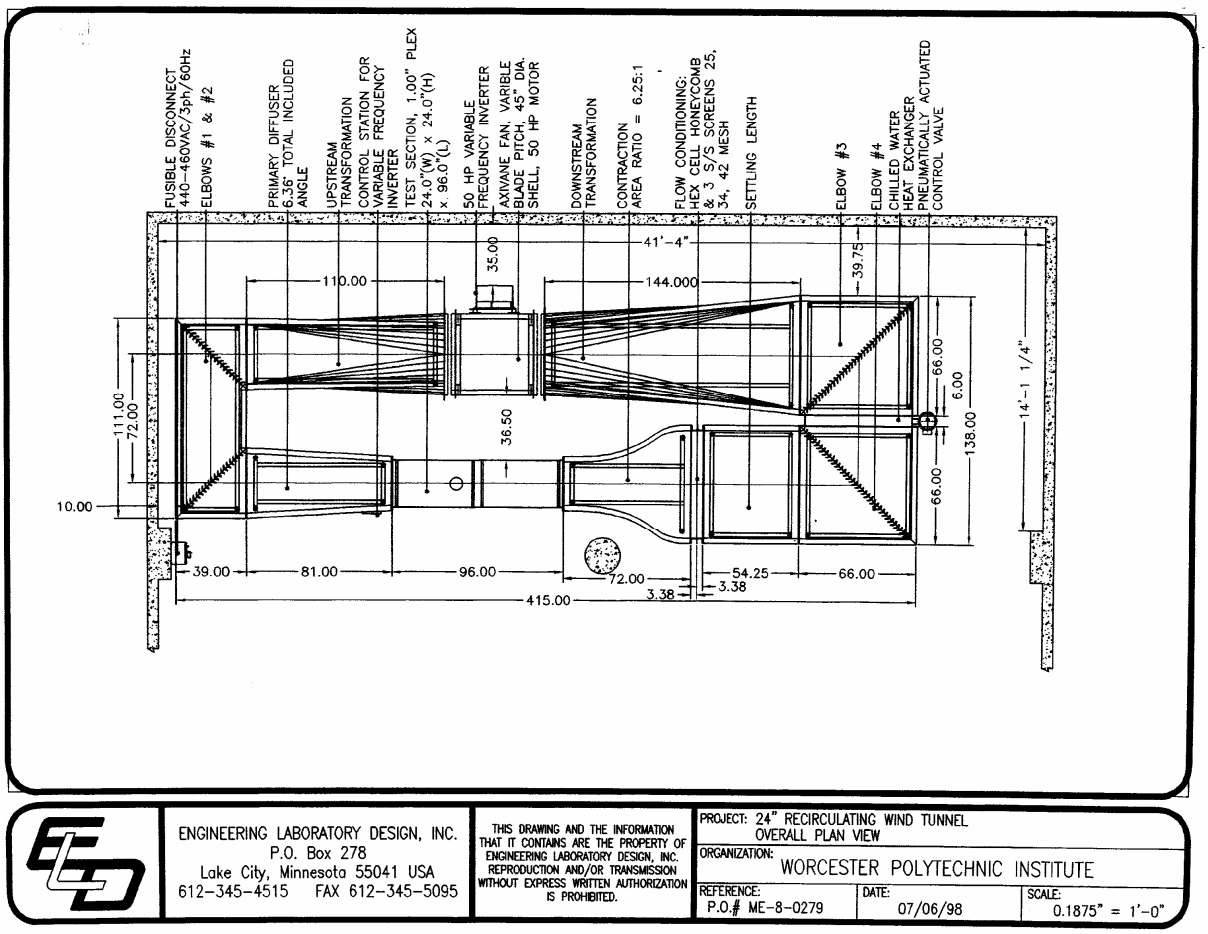

Figure 19: Closed Circuit Wind Tunnel. (From Engineering Laboratory Design [2], 1997)

In order to determine which velocity would be appropriate to run the wind tunnel at for our testing purposes, Reynolds number scaling was utilized. The Reynolds number is a non dimensional number relating viscous forces given by:

$$\mathrm{Re} = \frac{\rho V_\infty L}{\mu} = \frac{V_\infty L}{\nu} \quad (13)$$

where ρ is the density, μ is the dynamic fluid viscosity, L is the characteristic length and ν is the kinematic fluid viscosity. Preliminary Reynolds number scaling of our canopy resulted in a necessary wind tunnel velocity of more than 170m/s which is outside of the feasible velocity range. We then looked into scaling the Reynolds number according to a Re vs. C_d

graph of a flat disk or cup shape in free stream flow where C_d is the drag coefficient and can be found by:

$$C_d = \frac{D}{qA} \quad (14)$$

These results were found in Hoerner, 1958, and can be seen below.

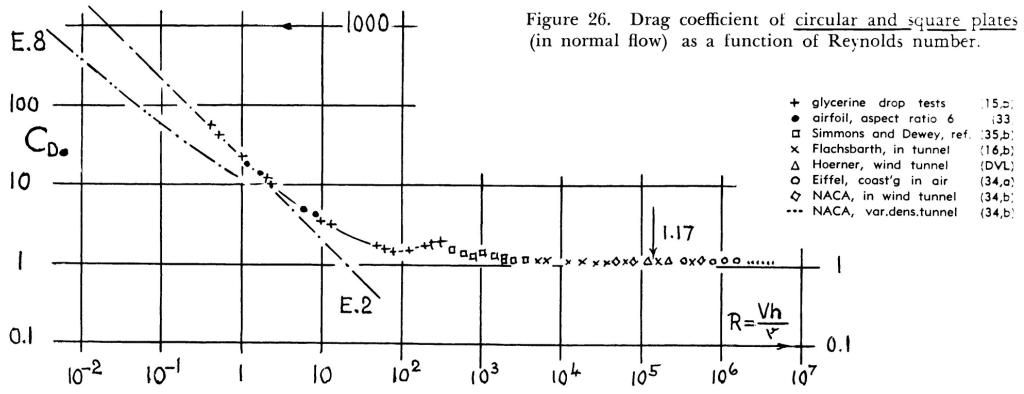

Figure 20: Reynolds Number vs. Drag Coefficient for a flat, circular disk

As you can see in Figure 20, there is a relatively horizontal section between Reynolds numbers of 10^3 and 10^6 which shows that the Cd is fairly constant over a wide range of velocities. Utilizing this information, we were able to choose a smaller velocity to run the wind tunnel at without significantly changing the drag coefficient that the parachute would produce. The velocities of 10m/s, 18m/s and 25m/s were The Reynolds numbers for these velocities are 1.47×10^5, 2.56×10^5 and 3.68×10^5 respectively. These Re values fall within the horizontal section on the Re vs. Cd plot.

For our lift and drag measurements, an Engineering Design Laboratory Inc. force balance was initially used. The force balance is a two component device which mounts on the outside of the bottom of the test section (E.L.D. [2], 1997). A hole has been drilled in the

Plexiglas bottom of the test section to allow the probe to extend into the section for connection to a test apparatus.

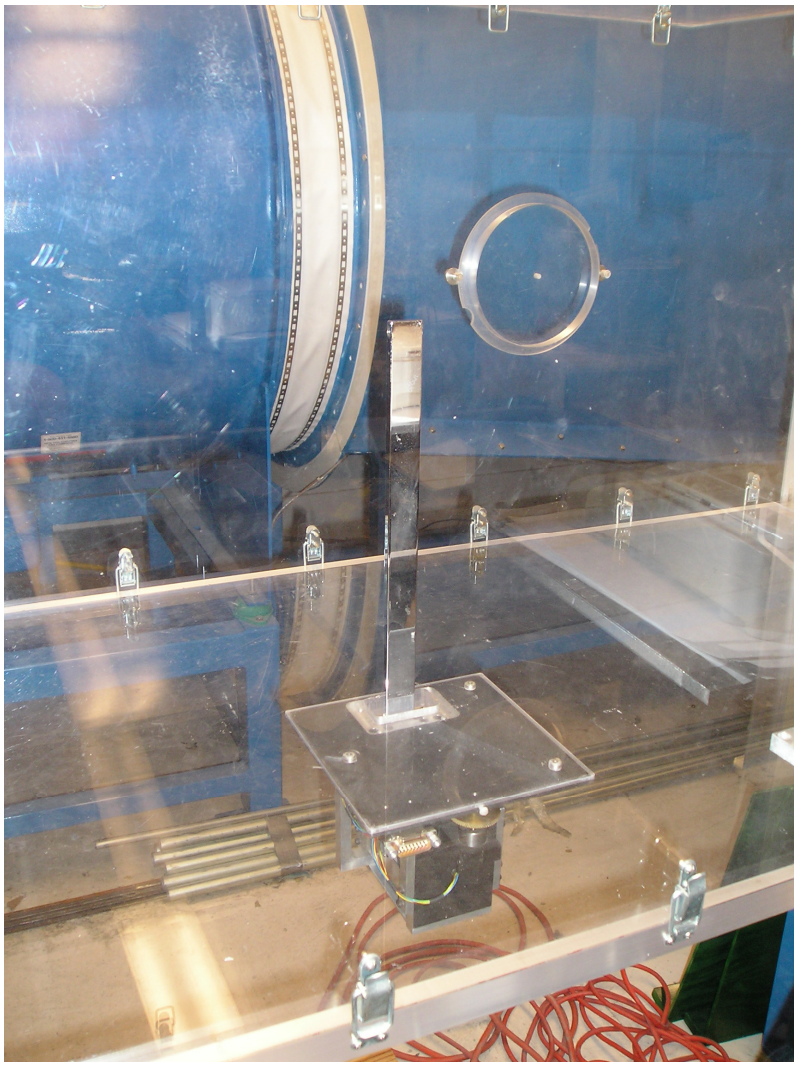

Figure 21: Dynamometer setup in wind tunnel

A model placed on the strut will then result in a deflection of the probing beam. These deflections are proportional to the forces applied on the test apparatus (E.L.D [2], 1997). These forces can be read using a calibration plot, which will be further described in subsequent sections. A diagram of the force dynamometer taken from E.L.D. [2], 1997, can be seen below.

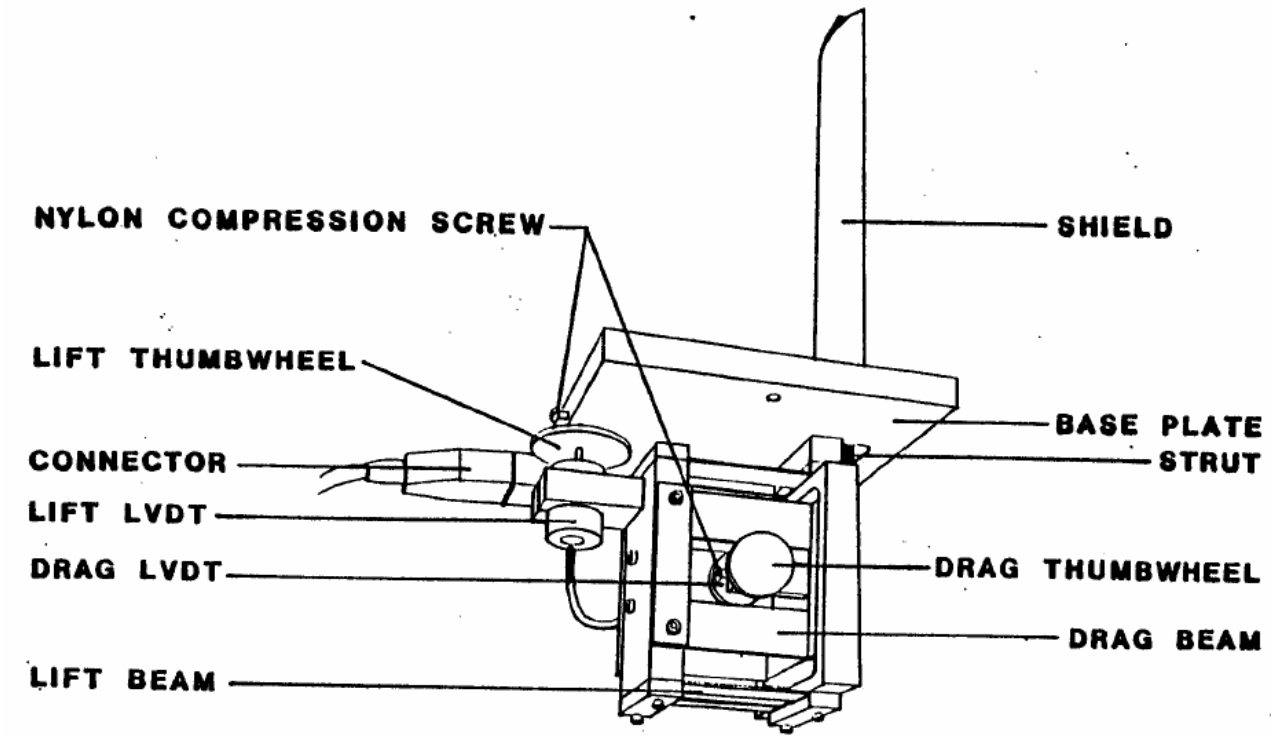

Figure 22: E.L.D Force Dynamometer. (From Engineering Laboratory Design [2], 1997)

For the purposes of this study, the airfoil shaped shield covering the beam has been removed. It has been determined (in previous studies) that the shield can skew results when running the tunnel by shifting slightly and possibly touching the beam itself. For the purposes of our experiments, it has been decided that the slight increase in vortex shedding from the dynamometer beam will have a smaller effect on measurements than the possible movement of the beam shield. For these reasons, the shield has been discarded during these experiments.

The final piece of hardware which was utilized in our testing was an E.L.D meter cabinet. This cabinet contains a DC power supply, five DC voltage digital meters, two signal conditioner cards, and a pressure transducer. The readouts on the cabinet are given in calibrated engineering units (E.L.D [2], 1997). This cabinet was connected directly to the dynamometer through a wired connector. A diagram of readout cabinet can be seen below (figure from E.L.D. [2], 1997).

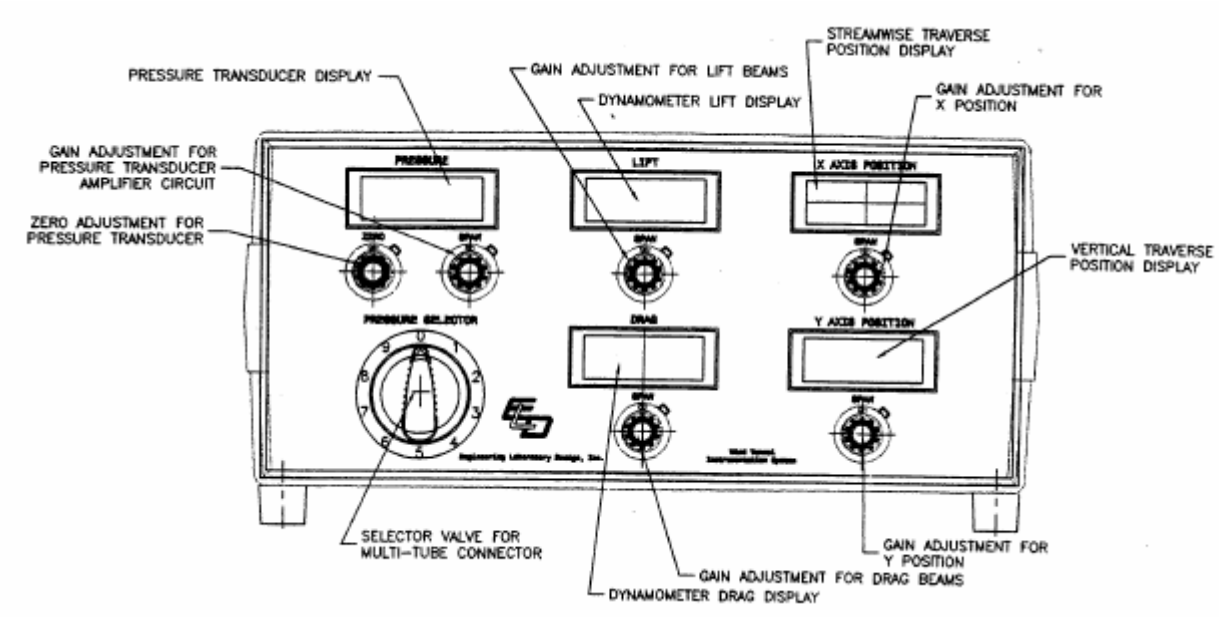

Figure 23: E.L.D Meter Cabinet

4.2 Dynamometer

4.2.1 Calibration

We needed to calibrate the dynamometer in order to get the proper results for our testing. Because the dynamometer only produces voltage readouts we needed to see how these compared to known forces. The easiest and most accurate way of doing this is to take masses and hang or place them on the dynamometer. We can simply place the dynamometer on a Plexiglas rig setup that orients the dynamometer sideways or upside down and allows masses to be hung off of it.

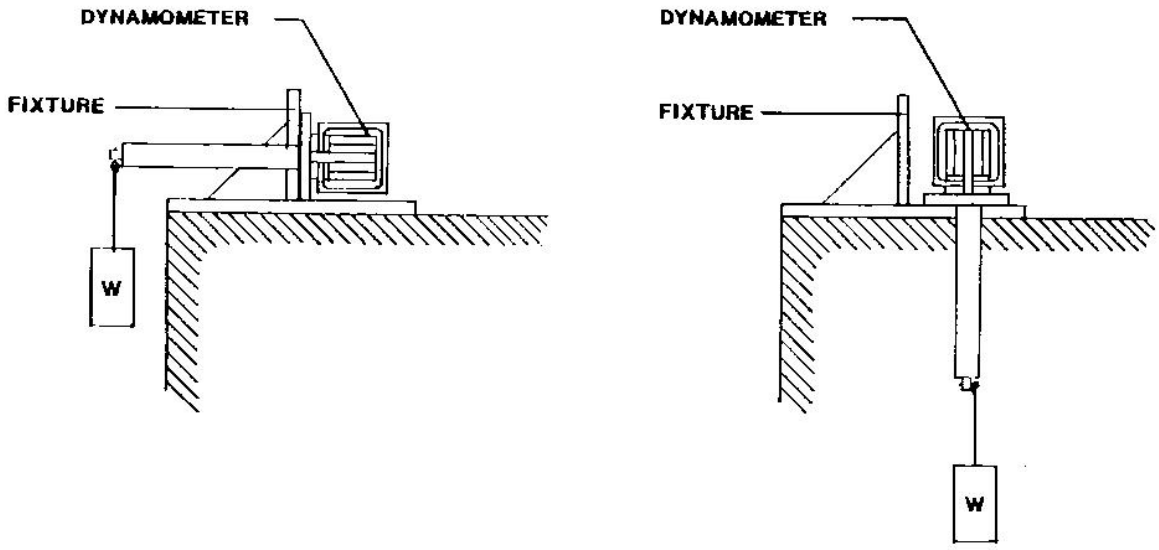

Figure 24: Orientation of the dynamometer for drag and lift calibration

The mass hangs straight down and thus records only a drag force on the dynamometer. The simple W = mg equation gives us the force and by taking multiple samples we can obtain a calibration graph. For our drag calibrations you can see the graph in Figure 25 below.

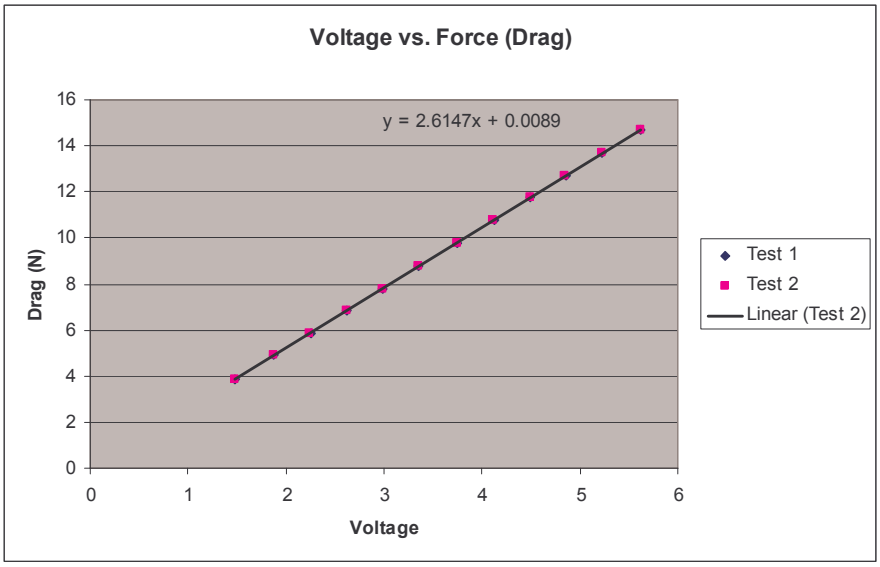

Figure 25: Drag Calibration Curve

This gives us an equation of:

$$D = 2.6147V + 0.0089 \quad (15)$$

Similarly we took readings for the lift force and shown in Figure 26 and Figure 27.

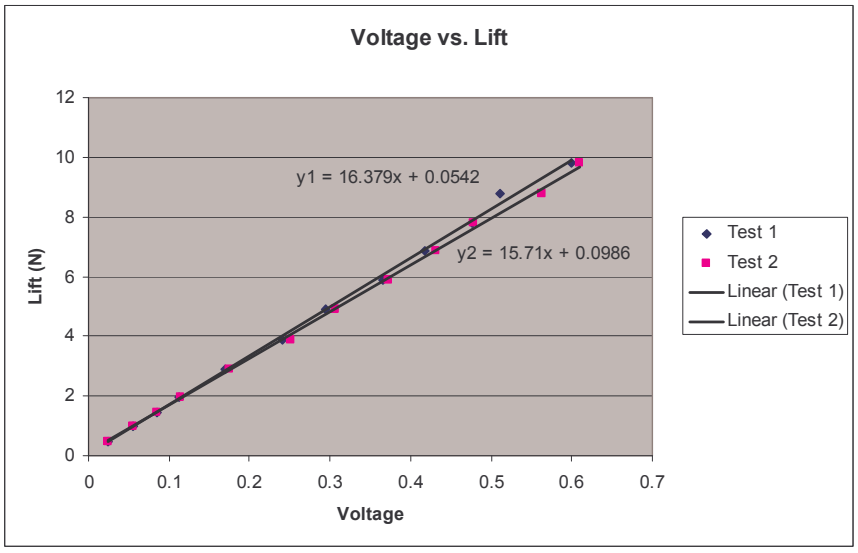

Figure 26: Lift Calibration Curves

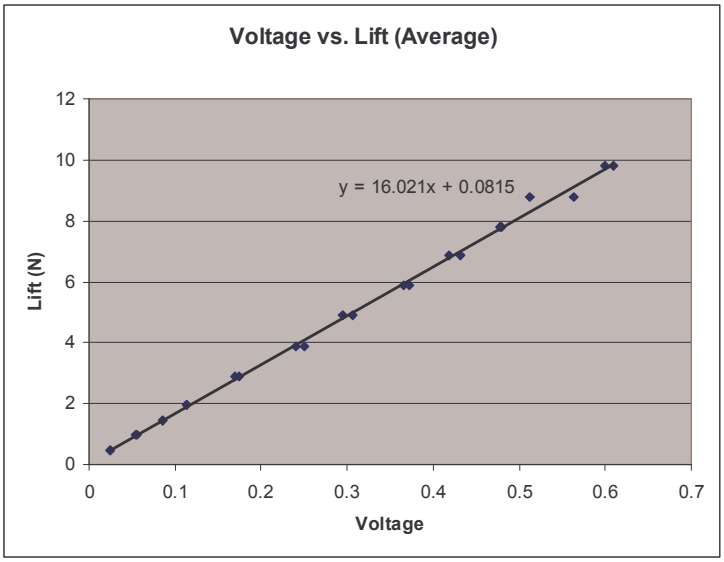

Figure 27: Mean Lift Calibration Curve

The lift equation we arrived at was:

$$L = 16.021V + 0.0815 \quad (16)$$

The data used to create these graphs can be found in Appendix B.

4.2.2 LabVIEW Data Acquisition

In order to get more accurate data, we chose to connect our dynamometer to LabVIEW. This allowed many points of data to be taken for one run and then averaged instead of reading points of off a digital display. We did this through the use of a DAQPad 6020-E. The back of the meter cabinet has an analog-out port with 15 pins which we used to connect to the DAQpad.

4.3 Six-Axis Transducer

4.3.1 Setup

After a first round of testing using the dynamometer, it was found that the resolution of the overall system, including that of the DAQ board, was not sufficient for measuring the small values of lift which were expected. For this reason, our setup was adapted to utilize a six-axis transducer along with attachment to both LabVIEW and Matlab for our force measurements.

The transducer which was used is manufactured by ATI Industrial Automation. The diagrams below show the setup of the transducer and its connection to the DAQ system as well as a detailed drawing of the transducer itself.

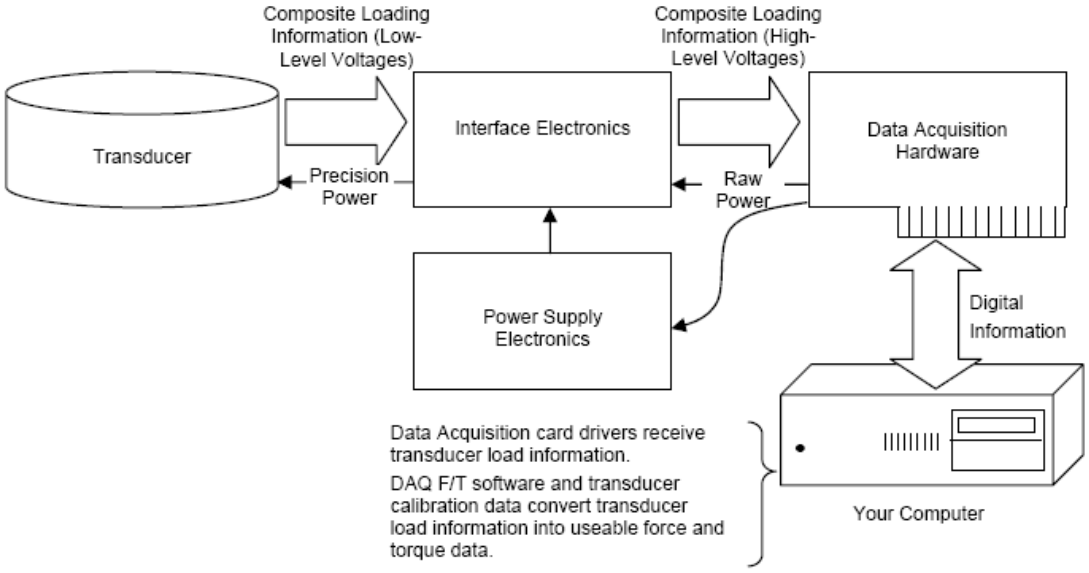

Figure 28: Setup of the Six-Axis Transducer

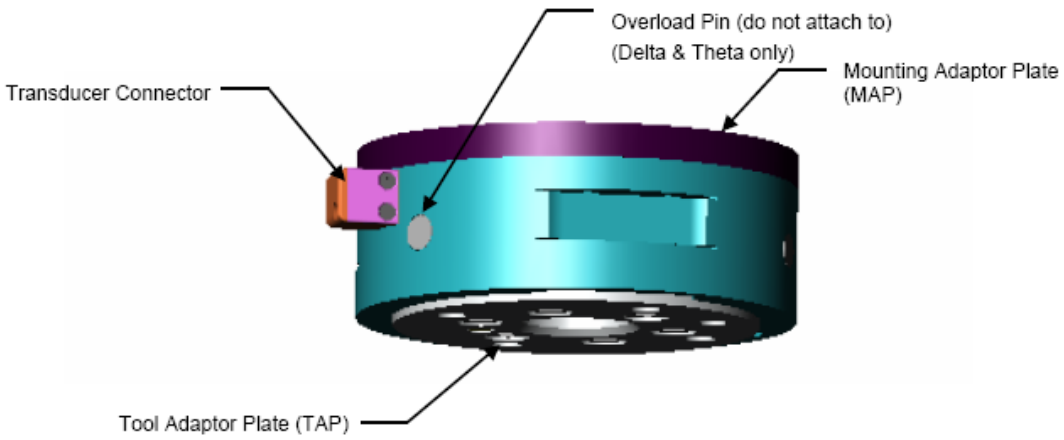

Figure 29: Drawing of Six-Axis Transducer

The transducer was mounted on an aluminum frame in order to allow for attachment of a sting to hold a test apparatus in the tunnel. A wooden frame was created in order to allow the structure to be mounted on top of the wind tunnel. This setup is shown in Figure 28.

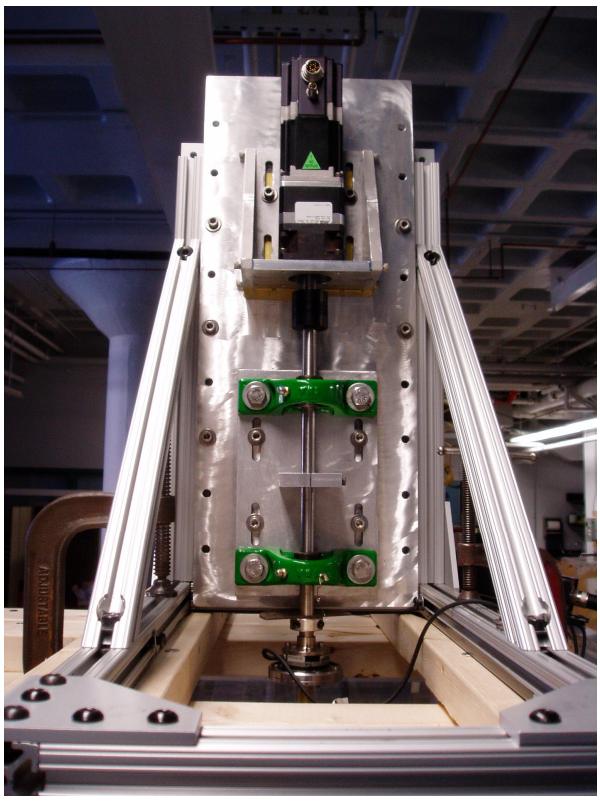

Figure 30: Transducer attached to frame and sting

4.3.1 Calibration and Alignment

Before testing with the six-axis transducer could begin, two alignments were necessary. First, the axis of measurement for the transducer needed to be properly aligned with the flow of the wind tunnel and held in place on the aluminum frame. This alignment was completed using the ATI test software provided by the Natick Army Soldier Center. A screenshot of this software can be seen in Figure 29.

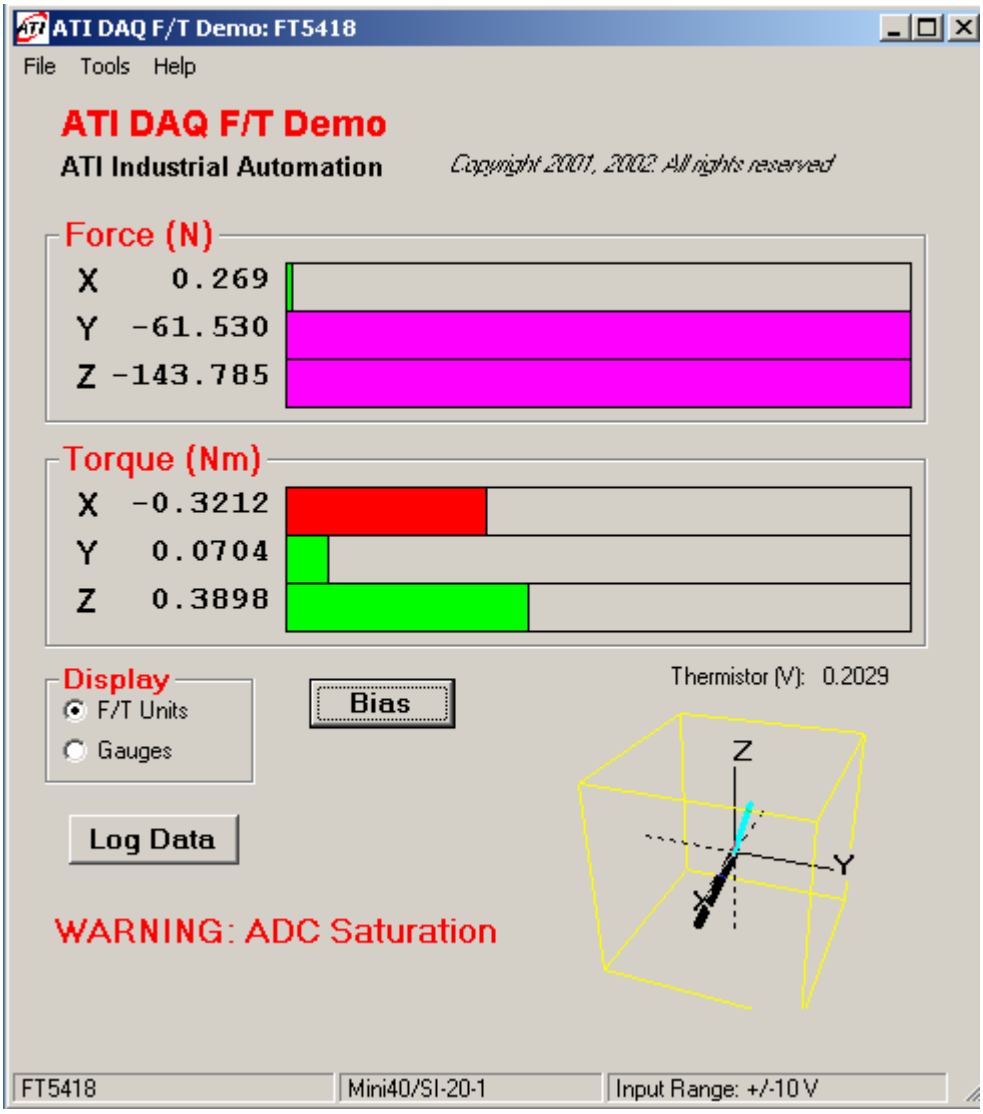

Figure 31: Screenshot of ATI DAQ F/T Demo Software

Utilizing this software, we were able to read the measurements of force and torque in each direction on the transducer at any given time. Attaching a string and pulley to the end of the sting in the direction of the wind tunnel flow allowed us to align the x-axis parallel to the flow of the tunnel. We then were able to check that the force perpendicular to the flow was being measured as the y-direction on the transducer. The x-axis of the transducer was used to measure drag while the y-axis was used in testing to measure the lift on the canopy as air flowed through the vents. The axis of the transducer can be seen in Figure 30.

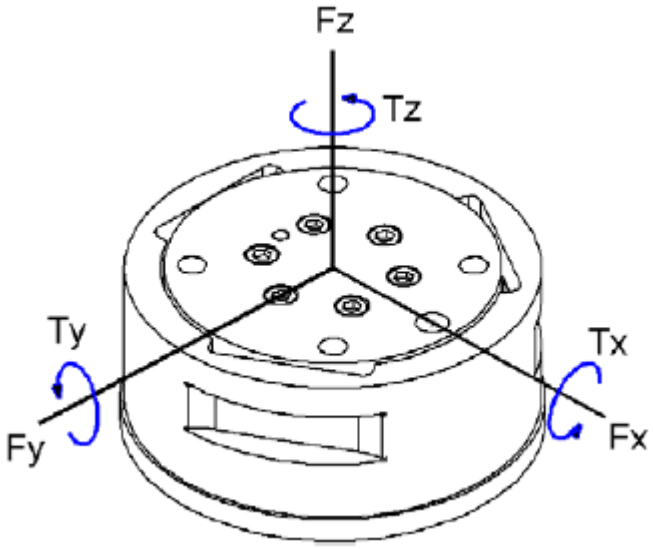

Figure 32: Directions of the Axis on the Transducer

The second alignment which had to be completed before testing could begin was to align the "L" shaped sting with the flow of the wind tunnel. This would assure that the canopy of the parachute would be oriented perpendicular to the flow. This was done by measuring the distance from each side of the wind tunnel to assure that the sting was correctly orientated. The sting and transducer were then tightened into place to assure that there would be no movement during testing.

A few simple calibration checks were completed before testing was started. In both the x and y directions, weights were placed on a pulley system with a string attachment to the sting. The force measured by the transducer was then read through the LabVIEW setup and compared to the theoretical force. The chart below shows the results of this calibration.

X-Direction Calibration			
Mass (kg)	**Expected Force (N)**	**Measured Force (N)**	**Offset (N)**
0.1	0.98	0.953	0.027
0.15	1.47	1.42	0.05
0.2	1.96	1.913	0.047

Table 2: X-Direction Calibration of Six Axis Transducer

Y-Direction Calibration			
Mass (kg)	**Expected Force (N)**	**Measured Force (N)**	**Offset (N)**
0.1	0.98	0.961	0.019
0.2	1.96	1.934	0.026

Table 3: Y-Direction Calibration of Six Axis Transducer

The findings of this calibration will be accounted for in the analysis of the results.

A similar calibration test was run with the solid apparatus attached to the sting. This calibration consisted of using the string-pulley-mass system in the y-direction and attaching the string to the ring of the solid structure. Using this method allowed us to apply the calibration force in the y-direction at the same location where the lift force caused by the flow actually acts. This would allow us to measure any bias in the data which was caused by the insertion of the structure into the system. The results of this calibration were as follows.

Y-Direction Calibration with Support Structure			
Mass (kg)	Expected Force (N)	Measured Force (N)	Offset (N)
0.1	0.98	0.756	0.224
0.15	1.47	1.152	0.318

Table 4: Y-Direction Calibration of Six-Axis Transducer Accounting for Support Structure

These findings will also be accounted for in the analysis of the results for the measurements of lift by applying a scale factor of 24% to the lift measurements.

A final calibration was completed in order to find the effect of the support structure on the measured drag of the canopy. This was done by placing the support structure in the wind tunnel without any canopy attached and measuring the baseline drag. The baseline drag was found to be .01594 N and will be subtracted from the measured drag in our final calculations.

4.3.2 Software

Two main software programs were utilized in order to gather the data from the six-axis transducer. The first was a LabVIEW program which collected the data at a selected sample rate and number of samples. This allowed us to control the rate at which our samples were collected and for how long. For these tests, the sample rate was set at 250 samples/sec (250 Hz) and over a period of 2 minutes. This means that 30,000 samples were taken during each test run. The large number of samples allowed us to minimize the effects of vibrations of the setup on the raw data. The LabVIEW software collected six sets of data for both force and torque in the x,y and z directions. For each of the canopies, three raw data tests were run at a velocity of 6.1 m/s (8Hz). A bias test was then run in order to remove the effects of the

mass of the canopy and support structure from the data. All the data was written to files with .lvm extensions. Below is a screenshot of the LabVIEW program which was utilized in our setup.

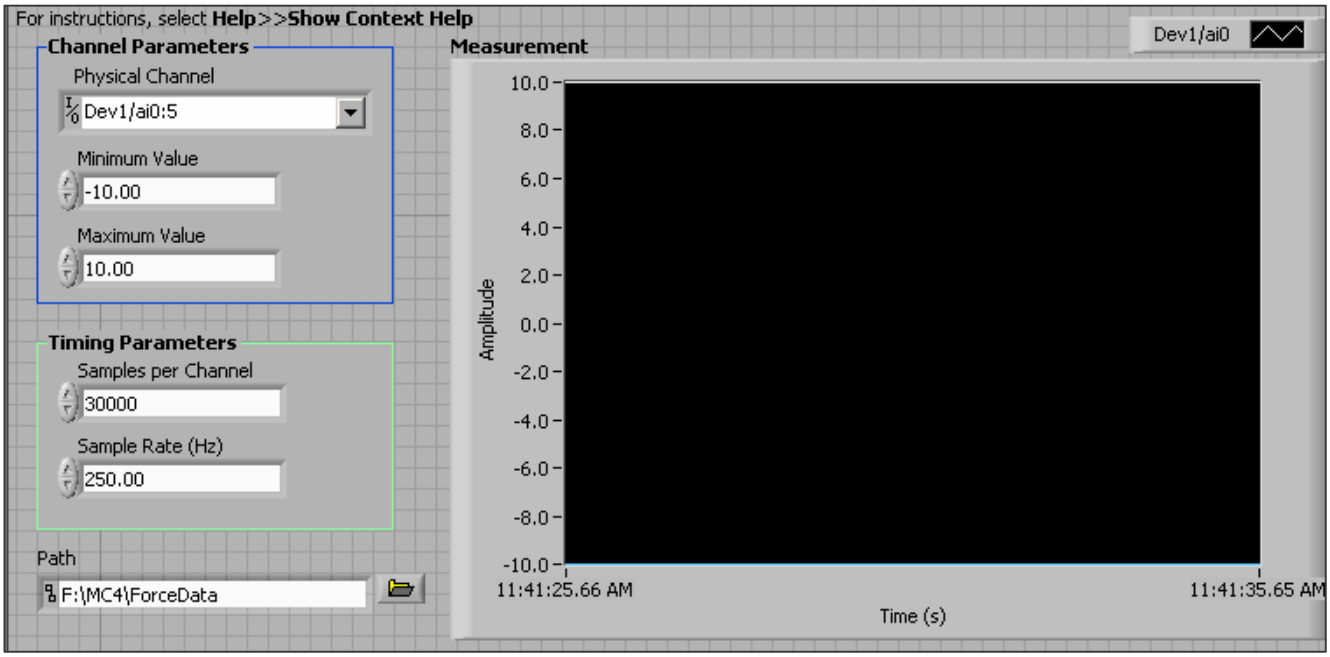

Figure 33: Screenshot of LabVIEW used to collect data

The second software program which was utilized was Matlab. Matlab was used to remove the bias information from the raw data which was collected for each of the canopies. The program which was used is titled *Conversion.m* and was created to subtract the thousands of bias data points from the raw data. Once the program was completed, the data was written to a text file and could be opened and analyzed in Microsoft Excel. Code for the *Conversion.m* program, as well as screenshots of its progression can be found in Appendix A.

4.4 Velocity Calibration

In order to calibrate the wind tunnel we acquired a digital manometer and a pitot tube which fit into the wind tunnel. The Setra Systems Model 264 manometer measures the difference between the static and stagnation pressures in inches of water. We ran the wind tunnel at 8 Hz (fan speed) and recorded the reading of .092 inches of water. From this we used the following equation to find the freestream velocity to be 6.1 m/s.

$$V_{\infty} = \sqrt{\frac{2 \cdot \rho_w \cdot g \cdot \Delta h}{\rho_{air}}} \quad (17)$$

5. Results

The results of this project encompassed a large amount of data distributed amongst many files and file types. Therefore, it was crucial to have a standard naming convention. The file names were all named as follows: Material type__ Vent Percentage__ Wind Tunnel Frequency__Test Number. For example, the data file for running the second test of a non-porous 4% canopy at 8Hz would be named NP_4_8Hz_Test2.ext, where ext stands for the necessary file extension. Once the data had been run through Matlab as described in Section 4.3.2, we took averages of the lift and drag for each test.

As you will see in the data chart below, it was necessary to correct the first set of data due to calibration offset. Initially we had checked the calibration of the y-axis by hanging a string off of the center of the sting. This calibration was consistent with the manufacturer's calibrations. However, because the support structure held the canopy so far from the sting, it was decided that the y-axis where the canopy would actually be placed needed to be tested. The results of this calibration can be seen in Section 4.3.1. The lift recorded was approximately 24% smaller than it should have been and thus resulted in a $\frac{100}{76}$ correction factor. In other words, the initial data divided by the correction factor gave us our new data. We also needed a correction factor of $\frac{100}{95}$ for the x-axis and corrected that data as well.

There was also an additional correction factor to account for the drag of the support structure. This had the effect of raising the glide ratio, however the magnitude of the increase was not very significant. The data was compiled into the data chart seen below in Table 5.

Canopy Type	Vent Area	Test Number	Force (N)						Cl	Cd	L/D
			8Hz (6.1 m/s)		8Hz - Corrected		Corrected for Drag				
			Drag	Lift	Drag	Lift	Drag	Lift			
Porous	control	1	1.586	0.046	1.669	0.061					
		2	1.586	0.042	1.669	0.055					
		3	1.585	0.035	1.668	0.046					
		average	**1.586**	**0.041**	**1.669**	**0.054**	**1.510**	**0.054**	**0.062**	**1.742**	**0.035675**
	6	1	1.618	0.206	1.703	0.271					
		2	1.628	0.208	1.714	0.274					
		3	1.621	0.212	1.706	0.279					
		average	**1.622**	**0.209**	**1.708**	**0.275**	**1.548**	**0.275**	**0.317**	**1.787**	**0.177329**
	8	1	1.606	0.203	1.691	0.267					
		2	1.612	0.210	1.697	0.276					
		3	1.619	0.208	1.704	0.274					
		average	**1.612**	**0.207**	**1.697**	**0.272**	**1.538**	**0.272**	**0.314**	**1.775**	**0.177088**
	10	1	1.607	0.311	1.691	0.409					
		2	1.612	0.328	1.696	0.432					
		3	1.615	0.319	1.700	0.420					
		average	**1.611**	**0.319**	**1.696**	**0.420**	**1.537**	**0.420**	**0.485**	**1.773**	**0.273496**
	12	1	1.595	0.342	1.679	0.450					
		2	1.596	0.351	1.680	0.462					
		3	1.600	0.348	1.684	0.458					
		average	**1.597**	**0.347**	**1.681**	**0.457**	**1.522**	**0.457**	**0.527**	**1.756**	**0.300055**
	14	1	1.588	0.406	1.672	0.534					
		2	1.595	0.413	1.679	0.543					
		3	1.600	0.409	1.684	0.538					
		average	**1.594**	**0.409**	**1.678**	**0.539**	**1.519**	**0.539**	**0.622**	**1.753**	**0.354609**
Non-Porous	control	1	1.601	0.013	1.685	0.017					
		2	1.604	0.023	1.688	0.030					
		3	1.613	0.021	1.698	0.028					
		average	**1.606**	**0.019**	**1.691**	**0.025**	**1.531**	**0.025**	**0.029**	**1.767**	**0.016242**
	2	1	1.714	0.050	1.804	0.066					
		2	1.712	0.056	1.802	0.074					
		3	1.711	0.048	1.801	0.063					
		average	**1.712**	**0.051**	**1.802**	**0.068**	**1.643**	**0.068**	**0.078**	**1.896**	**0.041084**
	4	1	1.645	0.074	1.732	0.097					
		2	1.663	0.075	1.751	0.099					
		3	1.659	0.088	1.746	0.116					
		average	**1.656**	**0.079**	**1.743**	**0.104**	**1.583**	**0.104**	**0.120**	**1.827**	**0.065653**
	6	1	1.629	0.160	1.715	0.211					
		2	1.626	0.159	1.711	0.210					
		3	1.630	0.165	1.716	0.217					
		average	**1.628**	**0.162**	**1.714**	**0.213**	**1.555**	**0.213**	**0.245**	**1.794**	**0.136744**
	8	1	1.650	0.163	1.737	0.214					
		2	1.655	0.195	1.742	0.257					
		3	1.659	0.193	1.747	0.253					
		average	**1.655**	**0.183**	**1.742**	**0.241**	**1.583**	**0.241**	**0.279**	**1.826**	**0.152516**
	10	1	1.640	0.278	1.727	0.366					
		2	1.633	0.287	1.719	0.378					
		3	1.632	0.297	1.718	0.391					
		average	**1.635**	**0.288**	**1.721**	**0.378**	**1.562**	**0.378**	**0.437**	**1.802**	**0.242306**

Table 5: Data Chart of Results

The first column of the data chart is the canopy material. The two types of material are then broken down into vent areas which are found in column two. Each number in the second column corresponds to the percentage of total area that is vented, while the control corresponds to no vent area. The third column is the test number and each vent area had 3

tests which were then averaged. The next two columns show the raw data from each of the tests. As already mentioned above, data correction was necessary, so the two columns after the raw data show our final corrected data. From the corrected data we were able to show the L/D ratios and lift and drag coefficients. From this data chart, we were able to produce the graphs seen below.

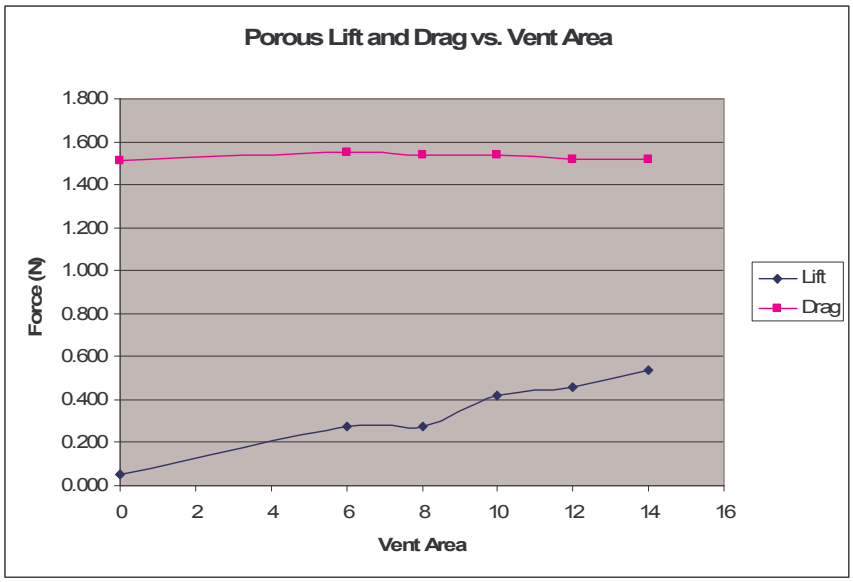

Figure 34: Lift and Drag vs. Vent Area for a Porous Canopy

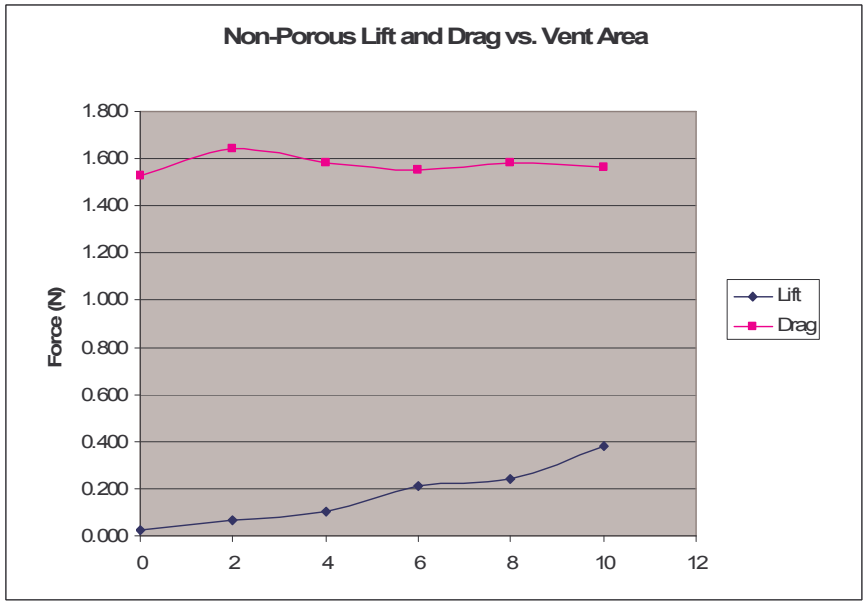

Figure 35: Lift and Drag vs. Vent Area for a Non-Porous Canopy

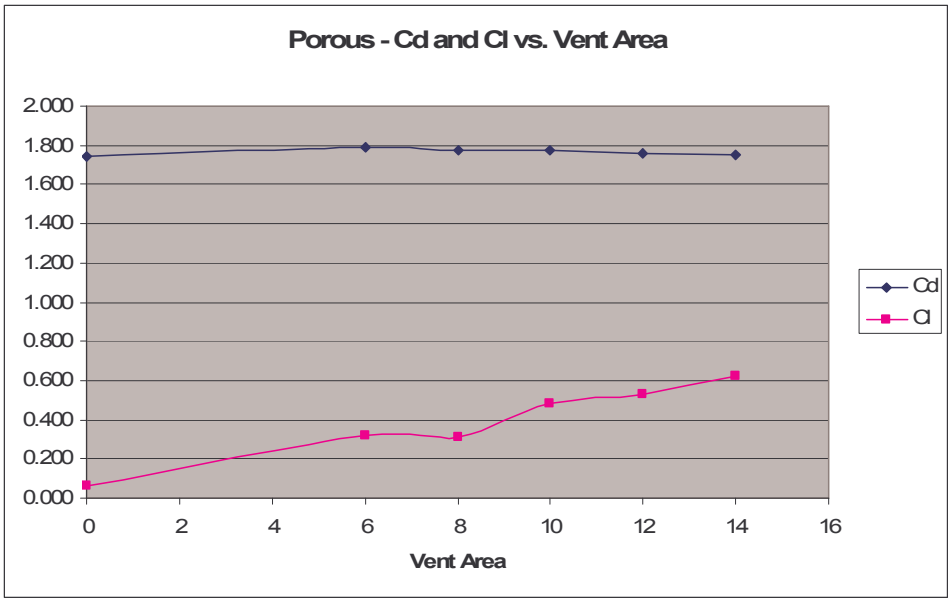

Figure 36: Lift and Drag Coefficients vs. Vent Area for a Porous Canopy

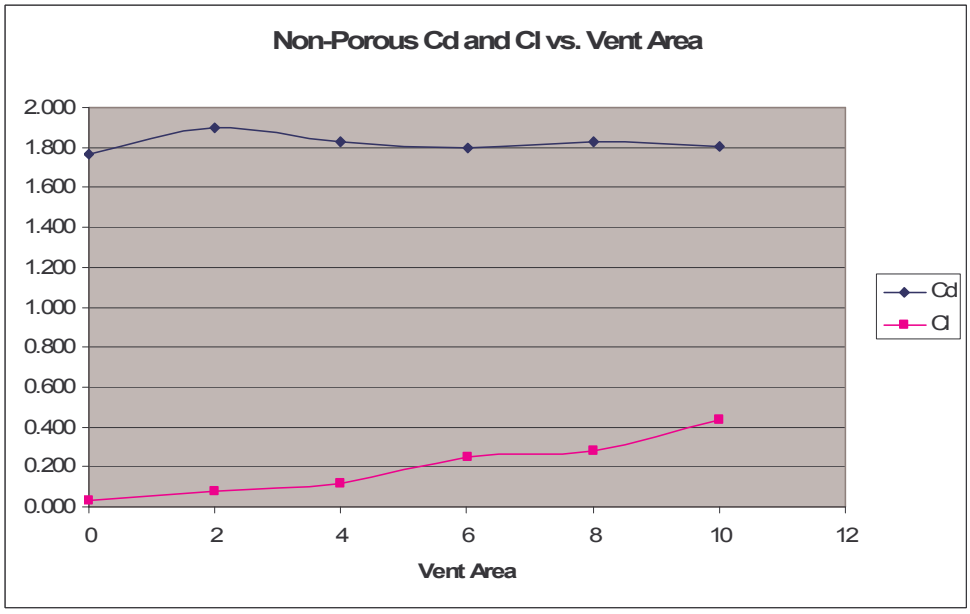

Figure 37: Lift and Drag Coefficients vs. Vent Area for a Non-Porous Canopy

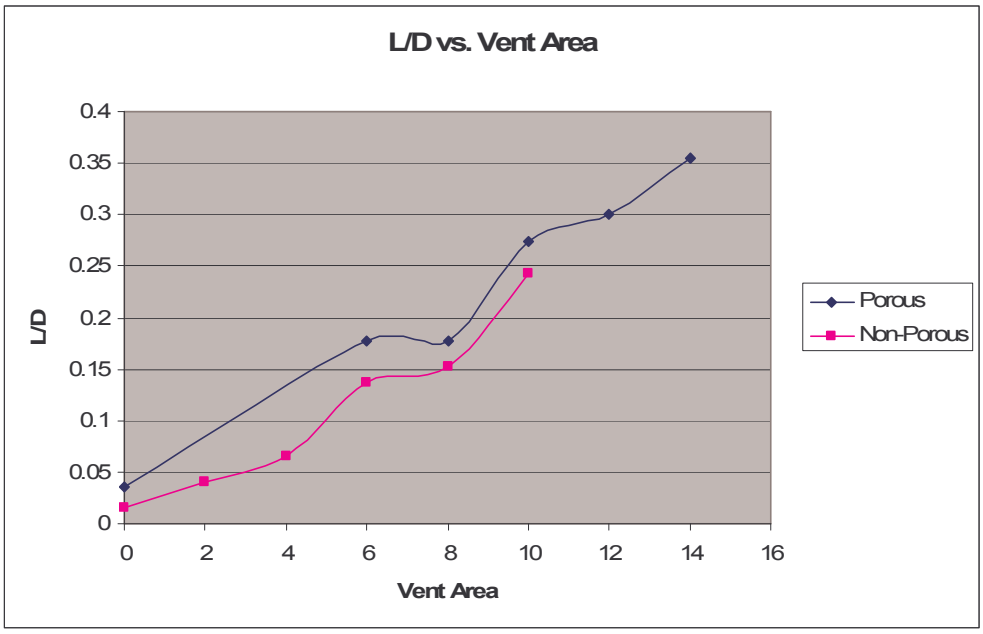

Figure 38: L/D ratio vs. Vent area for Porous and Non-Porous Canopies

6. Conclusions

The results of our testing indicate that lift coefficient and glide ratio will continually increase as vent area increases. However this is only valid for the range tested and should not be assumed to hold true for larger vent areas. These results contradict what we were expecting to see in the beginning of this project. We were expecting to find a peak in the lift coefficient and glide ratio graphs that would lead to an optimal vent area. Our guess of the peak occurring at 10% for porous and 6% for non-porous directly determined the sizes of the vent areas we tested. Another difference was the magnitude of our glide ratio and lift coefficients. In Lee, (2004) they measured a glide ratio of approximately 0.8 by dropping actual parachutes. The highest glide ratio we were able to obtain was 0.32, which is substantially lower.

The discrepancies between the actual results and the expected results may be caused in part by the angle of the flow entering the canopy. In these tests the airflow was perpendicular to the opening of the canopy. Due to this the air traveling through the vents tends to flow in the same direction as the freestream flow. The airflow area of each vent is also reduced by the angle at which the freestream flow enters the vent. In reality a vented parachute would glide through the air and would always have a horizontal (with respect to the earth's surface) velocity component. Because of this horizontal component of flow, the flow faces a larger vent area and this flow already has a horizontal component that helps create more lift for the parachute. These differences are likely the reason why our lift coefficients and glide ratios are relatively low compared to other experiments. A reason we did not find a peak could be because the flow angle reduced our effective vent area sizes and the peak may happen at a larger vent size.

7. Recommendations

As this project comes to its conclusion, we see many possibilities for future study in the area of vented round parachutes. Our results show that placing a vented round canopy in a directly perpendicular flow is not entirely representative of the freestream velocity seen by a falling canopy. For this reason, we recommend that a study be done with the canopy oriented at an angle to the freestream flow. This will allow a greater amount of air to flow through the vents, utilizing more vent area in each canopy. Since a full-scale canopy descending through the air would glide horizontally, this flow will be more representative of an actual canopy test.

We also recommend that test be run with a more rigid wind tunnel setup. This includes not only the support structure holding the canopies, but also the sting attached to the transducer. A more rigid setup would solve two issues which were raised in our testing. First, the canopy would not vibrate as much in the freestream flow, allowing for more accurate lift and drag measurements to be taken. Secondly, the structure would be able to withstand a higher freestream velocity while still producing accurate results. A higher velocity flow would be more representative of a full-scale canopy falling through the air.

Due to the small size of our canopies, the height of the vents needed to be rather large in order to accommodate the vent area requirements. We suggest further testing on canopies with smaller vent heights in order to better represent full-scale vented parachutes. In order to do this, the size of the canopies themselves would need to be increased. Due to the effects of the blockage ratio, it is suggested that these tests take place in a wind tunnel with a larger test section.

References

Barrett, R., "Parachutes for Planes," *Milwaukee Journal Sentinel Online*, June 29, 2003.

Budzinski, W., "AIR-POL: Parachutes," *Air-Pol Online*, Anglo-Polish Enterprise AIR-POL Ltd., Poland, 1994.

Carrington, D., "Da Vinci's Parachute Flies," *BBC News Online*, June 27, 2000.

Cicolello, J., "Paratroopers of the 50's," *The Rakkasans 187th Airborne Regimental Combat Team Association*, C J Magro Publishing, 1998.

Crowell, C., "Jalbert's Parafoil: Multi-Cell Wing Type Aerial Device," United States Patent #3285546, Patented November 15, 1966, www.kites.com, Updated October 7, 1998.

Day, B., Field, M., and Gelito, J., "An Experimental Investigation of Aerodynamic Drag on a Round Parachute Canopy," Major Qualifying Project, Worcester Polytechnic Institute, 2006.

Desabrais, K., *Velocity Field Measurements in the Near Wake of a Parachute Canopy*, PhD Thesis, Worcester Polytechnic Institute, Worcester, MA, 2002.

Engineering Laboratory Design Inc., "24 Inch Recirculating Wind Tunnel", *Operating and Maintenance Instructions*, Department of Mechanical Engineering, Worcester Polytechnic Institute, Worcester, Massachusetts, Serial number 6486, July, 1998.

Engineering Laboratory Design Inc. [2], "Wind Tunnel Instrumentation System," *Installation, Operation, and Maintenance Instructions*, Lake City, MN, 1997.

Hoerner, S., Fluid Dynamic Drag, self-published, 1958.

Johari, H., Desabrais, K., "Vortex shedding in the near wake of a parachute canopy," *J. Fluid Mech.*, Volume 536, pp.185-207, Worcester Polytechnic Institute, Worcester, MA, 2005.

Knacke, T., Parachute Recovery Systems: Design Manual, Para Publishing, Santa Barbara, CA, 1992

Lee, C., Buckley, J., *Method for Steerable Clustered Round Parachutes*, Journal of Aircraft, Volume 41, Number 5, Pages 1191-1195, American Institute of Aeronautcs and Astronautics, Inc., September-October 2004.

Poynter, D., Turoff, M., "The Skydiver's Handbook," *United States Parachute Association*, Para Publishing, 8th edition, February 2000.

Rae, W., Pope, A., Low Speed Wind Tunnel Testing, 2nd edition, John Wiley and Sons Publishing, New York, 1984.

Appendix A

Matlab code for Conversion.m:

```
clear; clc;

% Read raw data
[file, path] = uigetfile('*.lvm', 'Select raw data file');
if file ~=0
    [t0, ai0, t1, ai1, t2, ai2, t3, ai3, t4, ai4, t5, ai5] = textread([path file],...
        '%f %f %f %f %f %f %f %f %f %f %f %f',...
        'headerlines', 22,...
        'delimiter', '\t');
    RawData = [ai0, ai1, ai2, ai3, ai4, ai5];
else
    return;
end

%Load BiasData Matrix
[file, path] = uigetfile('*.lvm', 'Select bias data file or cancel for none');
if file ~= 0;
    [Biast0, Biasai0, Biast1, Biasai1, Biast2, Biasai2, Biast3, Biasai3, Biast4, Biasai4, Biast5, Biasai5] = textread([path file],...
        '%f %f %f %f %f %f %f %f %f %f %f %f',...
        'headerlines', 22,...
        'delimiter', '\t');
    BiasData = [Biasai0, Biasai1, Biasai2, Biasai3, Biasai4, Biasai5];
    data = ATIDaqFT_Convert(RawData(:, 1:6), BiasData);
else
    data = ATIDaqFT_Convert(RawData(:, 1:6));
end


% Save data to a Matlab file
Data = [t0 data];
[file, path] = uiputfile('*.mat', 'Select file to save');
HeaderNames = {'Time (s)', 'Fx (N)', 'Fy (N)', 'Fz (N)', 'Tx (N-m)', 'Ty (N-m)', 'Tz (N-m)'};
save([path file], 'HeaderNames', 'Data');

% Save data to a text file
if(file~=0)
    file2 = [file '.txt'];
    titles = ['Time (s)\t', 'Fx (N)\t', 'Fy (N)\t', 'Fz (N)\t', 'Tx (N-m)\t', 'Ty (N-m)\t', 'Tz (N-m)\n'];
    fid = fopen([path file2], 'w');
    fprintf(fid, titles);
    fprintf(fid, '%f\t%f\t%f\t%f\t%f\t%f\n', Data');
    fclose(fid);
end
```

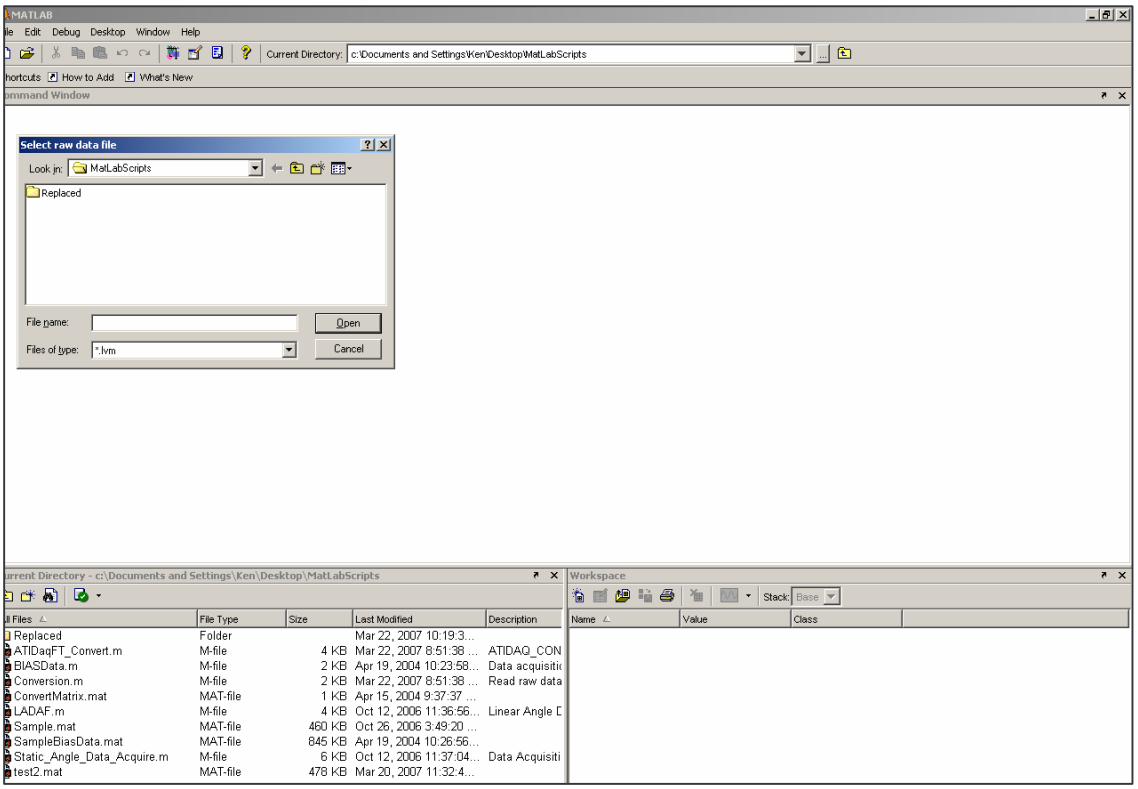

First Step of *Conversion.m*

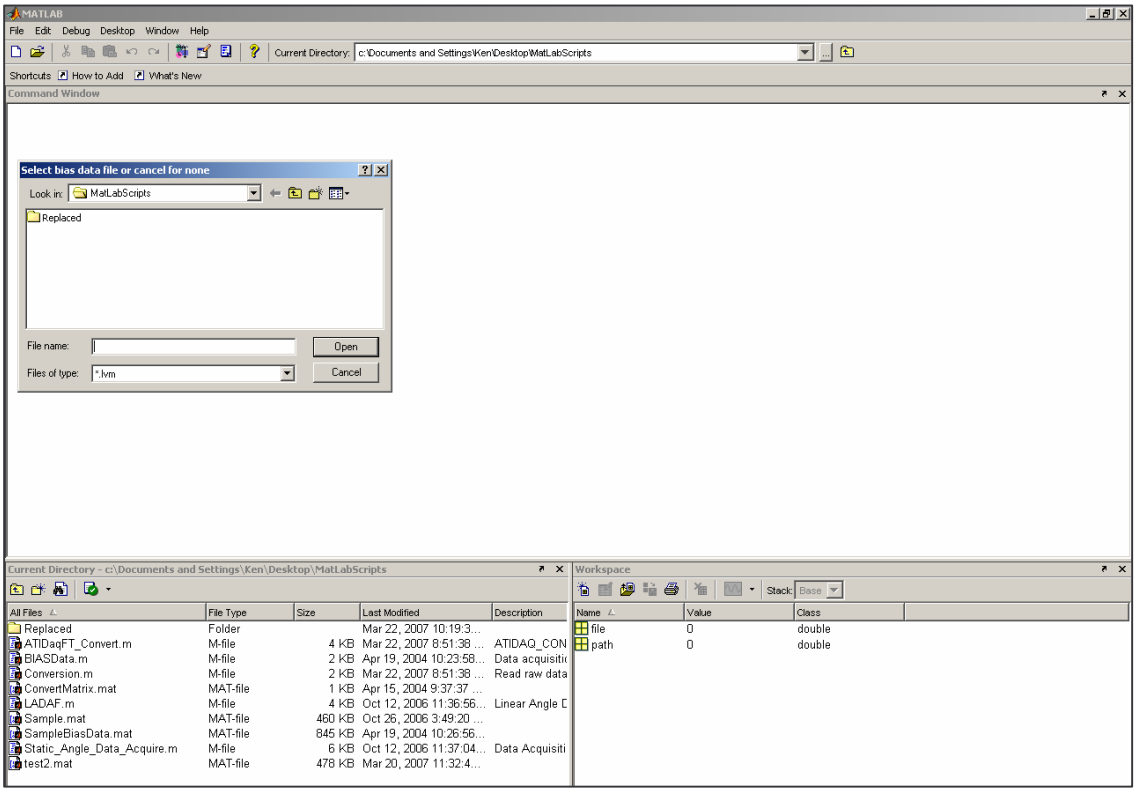

Second Step of *Conversion.m*

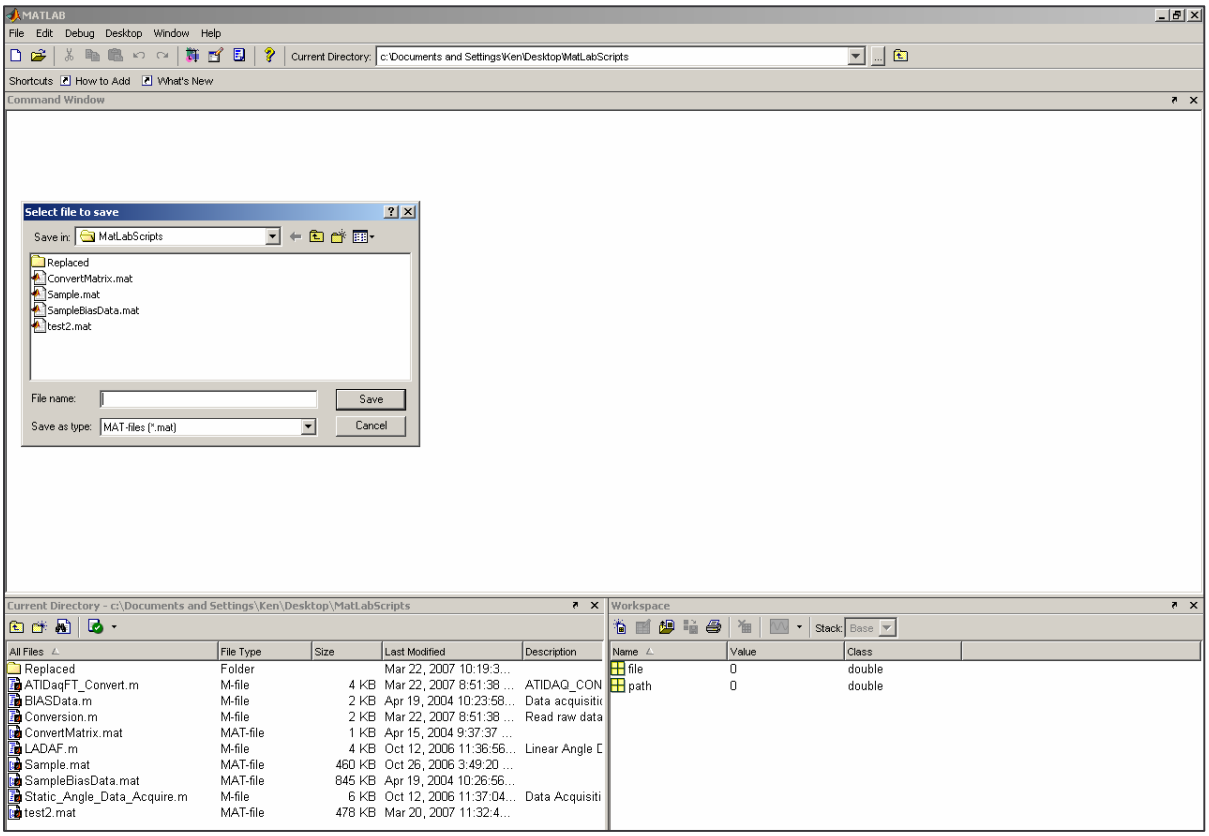

Final Step of *Conversion.m*

Appendix B

Lift and drag calibration data from force balance dynamometer:

Mass (kg)	Weight (N)	Drag -Volt (Run 1)	Drag -Volt (Run 2)
0.395	3.871	1.479	1.478
0.5	4.9	1.871	1.871
0.6	5.88	2.247	2.246
0.7	6.86	2.625	2.62
0.797	7.8106	2.988	2.983
0.895	8.771	3.353	3.35
1	9.8	3.744	3.744
1.1	10.78	4.122	4.119
1.2	11.76	4.498	4.495
1.295	12.691	4.854	4.85
1.395	13.671	5.229	5.225
1.5	14.7	5.622	5.62

Table 6: Drag Calibration

Mass	Weight (N)	Lift -Volt (Run 1)	Lift -Volt (Run 2)
0.05	0.49	0.025	0.025
0.1	0.98	0.056	0.055
0.147	1.4406	0.085	0.085
0.2	1.96	0.113	0.114
0.295	2.891	0.17	0.175
0.395	3.871	0.241	0.251
0.5	4.9	0.295	0.306
0.6	5.88	0.365	0.372
0.7	6.86	0.418	0.431
0.795	7.791	0.477	0.479
0.895	8.771	0.512	0.563
1	9.8	0.6	0.61

Table 7: Lift Calibration